

NAVAL POSTGRADUATE SCHOOL MONTEREY, CALIFORNIA



THESIS

**PREDICTION OF HYDRODYNAMIC
COEFFICIENTS UTILIZING GEOMETRIC
CONSIDERATIONS**

by

Eric P. Holmes

December, 1995

Thesis Advisor:

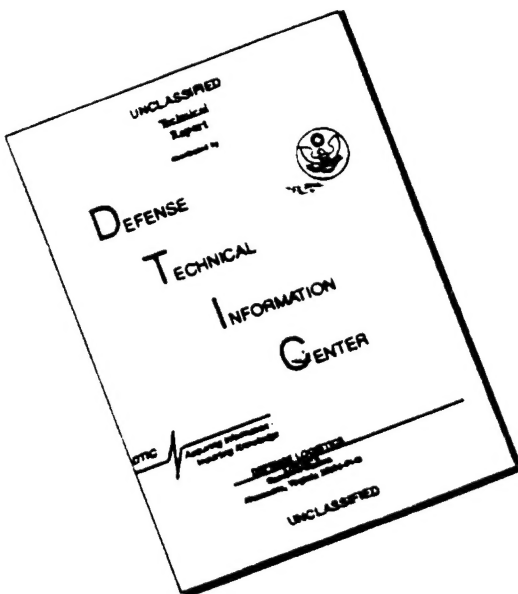
Fotis A. Papoulias

Approved for public release; distribution is unlimited.

19960405 095

DTIC QUALITY INSPECTED 1

DISCLAIMER NOTICE



THIS DOCUMENT IS BEST
QUALITY AVAILABLE. THE COPY
FURNISHED TO DTIC CONTAINED
A SIGNIFICANT NUMBER OF
PAGES WHICH DO NOT
REPRODUCE LEGIBLY.

REPORT DOCUMENTATION PAGE

Form Approved OMB No. 0704-0188

Public reporting burden for this collection of information is estimated to average 1 hour per response, including the time for reviewing instruction, searching existing data sources, gathering and maintaining the data needed, and completing and reviewing the collection of information. Send comments regarding this burden estimate or any other aspect of this collection of information, including suggestions for reducing this burden, to Washington Headquarters Services, Directorate for Information Operations and Reports, 1215 Jefferson Davis Highway, Suite 1204, Arlington, VA 22202-4302, and to the Office of Management and Budget, Paperwork Reduction Project (0704-0188) Washington DC 20503.

1. AGENCY USE ONLY (Leave blank)	2. REPORT DATE December 1995	3. REPORT TYPE AND DATES COVERED Master's Thesis
4. TITLE AND SUBTITLE PREDICTION OF HYDRODYNAMIC COEFFICIENTS UTILIZING GEOMETRIC CONSIDERATIONS		5. FUNDING NUMBERS
6. AUTHOR(S) Eric P. Holmes		
7. PERFORMING ORGANIZATION NAME(S) AND ADDRESS(ES) Naval Postgraduate School Monterey CA 93943-5000		8. PERFORMING ORGANIZATION REPORT NUMBER
9. SPONSORING/MONITORING AGENCY NAME(S) AND ADDRESS(ES)		10. SPONSORING/MONITORING AGENCY REPORT NUMBER
11. SUPPLEMENTARY NOTES The views expressed in this thesis are those of the author and do not reflect the official policy or position of the Department of Defense or the U.S. Government.		
12a. DISTRIBUTION/AVAILABILITY STATEMENT Approved for public release; distribution is unlimited.		12b. DISTRIBUTION CODE
13. ABSTRACT (maximum 200 words)		

A parametric study of a body of revolution is conducted utilizing existing semi-empirical methods for the calculation of hydrodynamic coefficients. The geometry of the body is analyzed in non-dimensional length and volume parameters. The effects of varying the nose, mid-body, and base fractions of the body on the hydrodynamic coefficients are generated and illustrated graphically. Equations for the hydrodynamic coefficients are then determined from the non-dimensional parameters. The results can be used to evaluate fundamental maneuvering characteristics early in the design phase.

14. SUBJECT TERMS Hydrodynamic coefficients, Computer modeling		15. NUMBER OF PAGES 94	
		16. PRICE CODE	
17. SECURITY CLASSIFICATION OF REPORT Unclassified	18. SECURITY CLASSIFICATION OF THIS PAGE Unclassified	19. SECURITY CLASSIFICATION OF ABSTRACT Unclassified	20. LIMITATION OF ABSTRACT UL

NSN 7540-01-280-5500

Standard Form 298 (Rev. 2-89)
Prescribed by ANSI Std. Z39-18 298-102

Approved for public release; distribution is unlimited.

**PREDICTION OF HYDRODYNAMIC COEFFICIENTS UTILIZING
GEOMETRIC CONSIDERATIONS**

Eric P. Holmes

Lieutenant Commander, United States Navy

B.S. Mathematics, SUNY at Binghamton, New York, 1978

M.B.A., Boston University, 1980

Submitted in partial fulfillment
of the requirements for the degree of

MASTER OF SCIENCE IN MECHANICAL ENGINEERING

from the

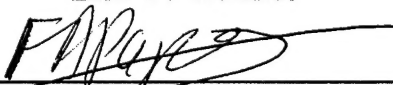
NAVAL POSTGRADUATE SCHOOL
December 1995

Author:

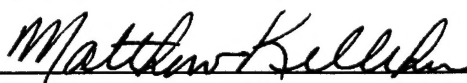


Eric P. Holmes

Approved by:



Fotis A. Papoulias, Thesis Advisor



Matthew D. Kelleher, Chairman

Department of Mechanical Engineering

ABSTRACT

A parametric study of a body of revolution is conducted utilizing existing semi-empirical methods for the calculation of hydrodynamic coefficients. The geometry of the body is analyzed in non-dimensional length and volume parameters. The effects of varying the nose, mid-body, and base fractions of the body on the hydrodynamic coefficients are generated and illustrated graphically. Equations for the hydrodynamic coefficients are then determined from the non-dimensional parameters. The results can be used to evaluate fundamental maneuvering characteristics early in the design phase.

TABLE OF CONTENTS

I.	INTRODUCTION.....	1
A.	GENERAL CONCEPTS.....	1
B.	PROGRAM APPLICATION.....	2
II.	DETERMINATION OF HYDRODYNAMIC COEFICIENTS.....	5
A.	THE GENERAL PHYSICAL DESCRIPTION.....	5
B.	HYDRODYNAMIC COEFFICIENT CALCULATION.....	9
C.	PROGRAM VALIDATION.....	12
III.	PARAMETRIC STUDY.....	15
A.	INTRODUCTION.....	15
B.	PHYSICAL REVIEW OF PARAMENTER MODIFICATIONS.....	16
C.	COMPUTER MODEL DEVELOPMENT.....	17
D.	HYDRODYNAMIC COEFFICIENT MESH GRAPHS.....	19
E.	VOLUME AND LENGTH VARIATIONS.....	36
IV.	DETERMINATION OF FUNCTIONAL COEFFICIENTS.....	45
A.	INTRODUCTION.....	45
B.	PREDICTION EQUATION.....	46
V.	CONCLUSIONS AND RECOMMENDATIONS.....	59
A.	CONCLUSIONS.....	59
1.	Summary Review of Parameter Variations.....	59
2.	Final Comparison.....	60
B.	RECOMMENDATIONS.....	60
	APPENDIX A. MATLAB ROUTINE FOR DETERMINING HYDRODYNAMIC COEFICIENTS WITH VARYING NOSE AND MID-BODY FRACTIONS.....	63
	APPENDIX B. SAMPLE MATLAB ROUTINE FOR DETERMINING THE FUNCTIONAL COEFICIENTS FROM A SURFACE PROFILE.....	79
	LIST OF REFERENCES.....	81
	INITIAL DISTRIBUTION LIST.....	83

LIST OF FIGURES

1. Overview of forces and velocities.....	1
2. Slice pod drawing.....	3
3. Geometric parameter description for body of revolution.....	5
4. S_v and S_{tb} illustration.....	8
5. Basic shape.....	16
6. Lower F_n and slenderness ratio (shorter and fatter).....	17
7. Higher F_n and lower F_b , higher slenderness ratio (slimmer).....	17
8. Lower F_n , higher F_m , lower F_b , constant slenderness ratio.....	17
9. Matrix interpretation for data analysis.....	19
10. Slenderness ratio mesh graph.....	21
11. Y_{vprime} standard scale mesh graph.....	22
12. N_{vprime} standard scale mesh graph.....	23
13. Y_{rprime} standard scale mesh graph.....	24
14. N_{rprime} standard scale mesh graph.....	25
15. $Y_{vdprime}$ standard scale mesh graph.....	26
16. $N_{vdprime}$ standard scale mesh graph.....	27
17. $N_{rdprime}$ standard scale mesh graph.....	28
18. Y_{vprime} close-up scale mesh graph.....	29
19. Y_{vprime} variations with mid-body fraction.....	29
20. N_{vprime} close-up scale mesh graph.....	30
21. N_{vprime} variations with mid-body fraction.....	30
22. Y_{rprime} close-up scale mesh graph.....	31
23. Y_{rprime} variations with mid-body fraction.....	31
24. N_{rprime} close-up scale mesh graph.....	32
25. N_{rprime} variations with mid-body fraction.....	32
26. $Y_{vdprime}$ close-up scale mesh graph.....	33
27. $Y_{vdprime}$ variations with mid-body fraction.....	33
28. $N_{vdprime}$ close-up scale mesh graph.....	34
29. $N_{vdprime}$ variations with mid-body fraction.....	34
30. $N_{rdprime}$ close-up scale mesh graph.....	35
31. $N_{rdprime}$ variations with mid-body fraction.....	35
32. Variation of V/L^3 ratio drawing.....	36
33. Y_{vprime} V/L^3 variations at 10% nose fraction.....	37
34. Y_{vprime} V/L^3 variations at 20% nose fraction.....	37

LIST OF FIGURES

35. Nvprime V/L^3 variations at 10% nose fraction.....	38
36. Nvprime V/L^3 variations at 20% nose fraction.....	38
37. Yrprime V/L^3 variations at 10% nose fraction.....	39
38. Yrprime V/L^3 variations at 20% nose fraction.....	39
39. Nrprime V/L^3 variations at 10% nose fraction.....	40
40. Nrprime V/L^3 variations at 20% nose fraction.....	40
41. Yvdprime V/L^3 variations at 10% nose fraction.....	41
42. Yvdprime V/L^3 variations at 20% nose fraction.....	41
43. Nvdprime V/L^3 variations at 10% nose fraction.....	42
44. Nvdprime V/L^3 variations at 20% nose fraction.....	42
45. Nrdprime V/L^3 variations at 10% nose fraction.....	43
46. Nrdprime V/L^3 variations at 20% nose fraction.....	43
47. Yvprime theoretical mesh graph.....	48
48. Yvprime predicted mesh graph.....	48
49. Nvprime theoretical mesh graph.....	49
50. Nvprime predicted mesh graph.....	49
51. Yrprime theoretical mesh graph.....	50
52. Yrprime predicted mesh graph.....	50
53. Nrprime theoretical mesh graph.....	51
54. Nrprime predicted mesh graph.....	51
55. Yvdprime theoretical mesh graph.....	52
56. Yvdprime predicted mesh graph.....	52
57. Nvdprime theoretical mesh graph.....	53
58. Nvdprime predicted mesh graph.....	53
59. Nrdprime theoretical mesh graph.....	54
60. Nrdprime predicted mesh graph.....	54
61. Yvprime equation percentage error.....	55
62. Nvprime equation percentage error.....	55
63. Yrprime equation percentage error.....	56
64. Nrprime equation percentage error.....	56
65. Yvdprime equation percentage error.....	57
66. Nvdprime equation percentage error.....	57
67. Nrdprime equation percentage error.....	58

I. INTRODUCTION

A. GENERAL CONCEPTS

Ships are designed to operate in a hostile environment. Even during peacetime the ship must navigate the water and arrive at its destination intact and ontime. The motion of the ship is affected by the presence of other ships, hazards to navigation, established traffic patterns, and the sea. The motion of the ship is directed and the track of the ship is plotted on the chart. The response of the ship to changes in speed and rudder commands is studied under standard assumptions of marine vehicle dynamics. The forces and moments subjected to the ship due to its relative motion in the water are the basis for this study. Figure 1 illustrates the basic concepts and definitions.

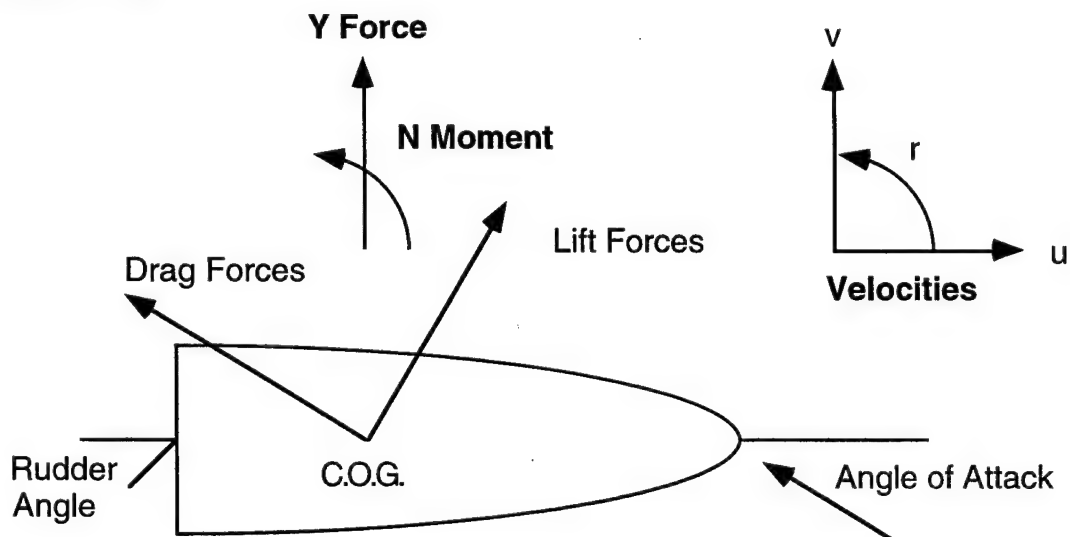


Figure 1. Overview of forces and velocities. [1]

The motion of the ship can be described in the global sense and in the body fixed reference frame. The body fixed reference frame is utilized in this study. The ship's velocity along its x axis is u . The sideslip velocity is v and the angular velocity is r .

When the water impacts the ship at an angle of attack, lift and drag forces are developed. These impart a lateral Y force and a pitching N moment. We can determine the lateral Y force resulting from a sideslip velocity v and an angular velocity r . We can determine the pitching N moment resulting from a slideslip velocity v and angular velocity r . In review of the effects of acceleration, \dot{v} and \dot{r} , these effects can be computed.

A measure of the ship's stability in design is its ability to maintain or regain straight line motion when forces act on its shape. The linearized models for equations of motion utilize hydrodynamic derivatives of the Y force and the N moment to describe their behavior. There are a number of mathematical methods for determining the hydrodynamic derivatives and LT Wolkerstofer [2] summarized them in his thesis. In our work, the semi-empirical methods that utilize the geometric considerations of a body of revolution, typical of a modern submarine are best suited for our purpose.

B. PROGRAM APPLICATION

The body of revolution that we shall consider is a basic submarine shape. The nose is elliptical, the mid-body is cylindrical,

and the base is conical. This is an approximate SUBOFF model [2] and it is also the shape of the slice pod which is illustrated in Figure 2.

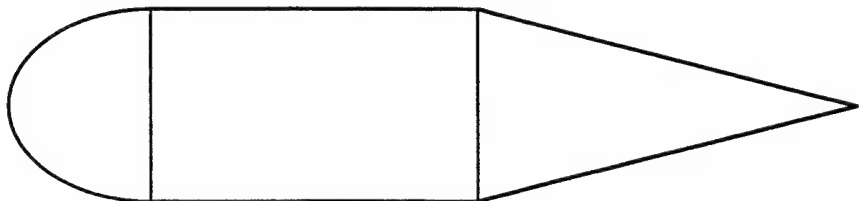


Figure 2. A body of revolution.

This axisymmetric shape is a simple model but the concepts applied to this model can be broadened to fit any shape. Our goal is to take a shape that has been tested and to modify its parameters to see how geometric changes effect the hydrodynamic derivatives which affect the stability and turning characteristics of the platform.

II. DETERMINATION OF HYDRODYNAMIC COEFFICIENTS

A. THE GENERAL PHYSICAL DESCRIPTION

The body of revolution consists of three main sections. The forward section is an ellipsoid, the mid-body section is a cylinder and the base section is a cone. This is the shape utilized for numerous studies and is the shape of the slice pod. The generic figure is illustrated in Figure 3.

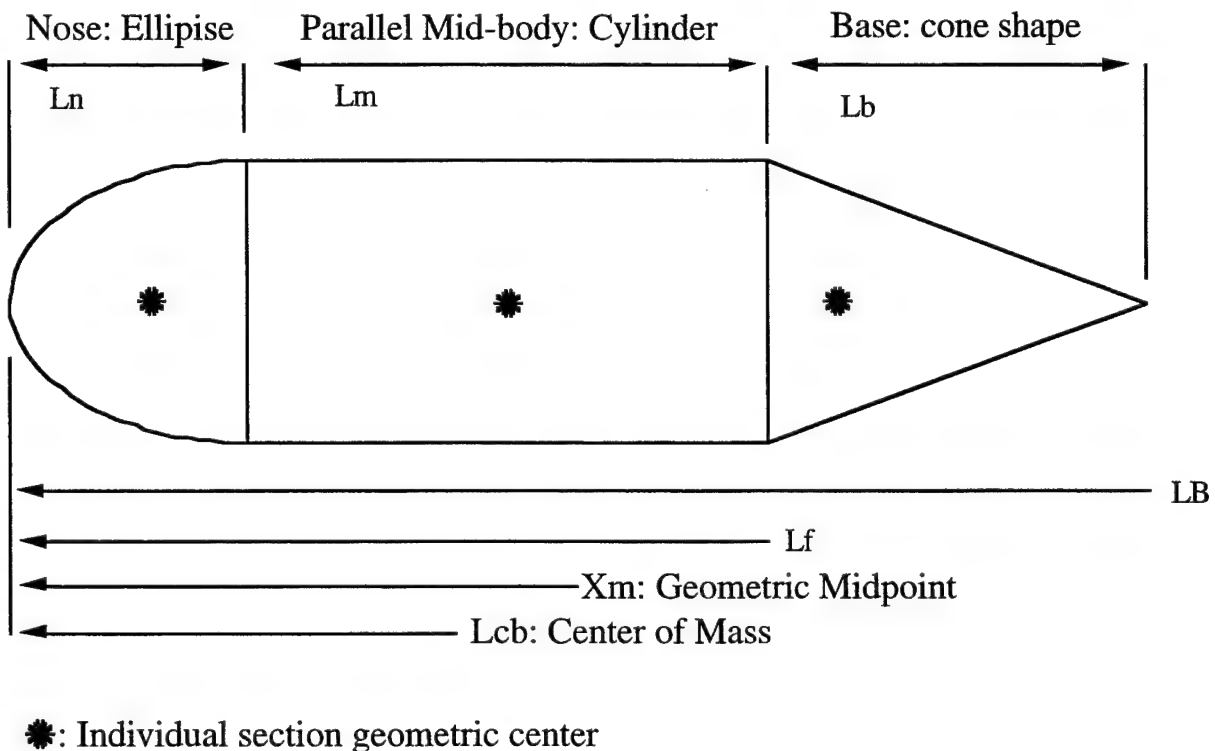


Figure 3. Geometric parameter description for body of revolution.

The various methods utilized for the estimation of hydrodynamic coefficients were compared by LT Wolkerstofer [2].

The body of revolution hydrodynamic coefficients depend on semi-empirical relations to account for the viscous or vortex effects on the body. The methods based primarily on geometric considerations are applied in this parametric study. The hydrodynamic coefficients will be determined from the United States Air Force Data Compendium (USAF DATCOM) method which is summarized by Peterson [3]. The acceleration hydrodynamic coefficients will be determined by the methods of Humpreys and Watkinson [4].

To initiate the parametric study we needed to non-dimensionalize a number of characteristics of the body of revolution. The lengths of each section of the body are described by the fractional amount of the total length as in the nose fraction.

$$F_n = \frac{l_n}{l_B} \quad (1)$$

The slenderness ratio is defined using the total length.

$$S = \frac{l_B}{d} \quad (2)$$

The volume the body of revolution would be determined from the sum of the three sections using standard volume formulas but with all the lengths referenced to the total length of the body via fractional amounts.

$$V = \left(\frac{\pi d^2 l_B}{12} \right) (2F_n + 3F_m + F_b) \quad (3)$$

From this relation it is clear that the mid-body fraction is the dominant term in determination of the volume amount. This is consistent with the realization that the mid-body diameter is the maximum diameter for the body and constant mid-body length. The determination of the volume is important because it is the volume which determines the buoyant forces resulting from the shape. A larger volume will have a larger buoyant force.

When the volume is non-dimensionalized the diameter of the body of revolution will be determined in the following relation.

$$d = \sqrt{(12V) / (\pi l_B)(2F_n + 3F_m + F_b)} \quad (4)$$

The geometric center of the body of revolution will depend on the lengths of the individual sections. We utilized standard formulas for each section to find the geometric center for each section and then combined then to determine the offset from the geometric midpoint of the mid-body section.

$$X_b = \left(\frac{\pi d^2}{12V} \right) \left[2l_n \left(\frac{l_m}{2} + \frac{3l_n}{8} \right) - l_b \left(\frac{l_m}{2} + \frac{3l_b}{4} \right) \right] \quad (5)$$

This offset from the center of the mid-body section is then applied to find the geometric center for the body which is the same as the center of buoyancy for the body in horizontal motion.

$$l_{cb} = l_n + \frac{l_m}{2} - X_b \quad (6)$$

The axial position where the flow becomes predominantly viscous is a function of the overall length determined from the point on the body of maximum slope [3]. The axial position, L_v is utilized for the determination of a few parameters affecting the hydrodynamic coefficients.

$$l_v = 0.905 \times l_B \quad (7)$$

The geometry of the body at L_v is illustrated in Figure 4.

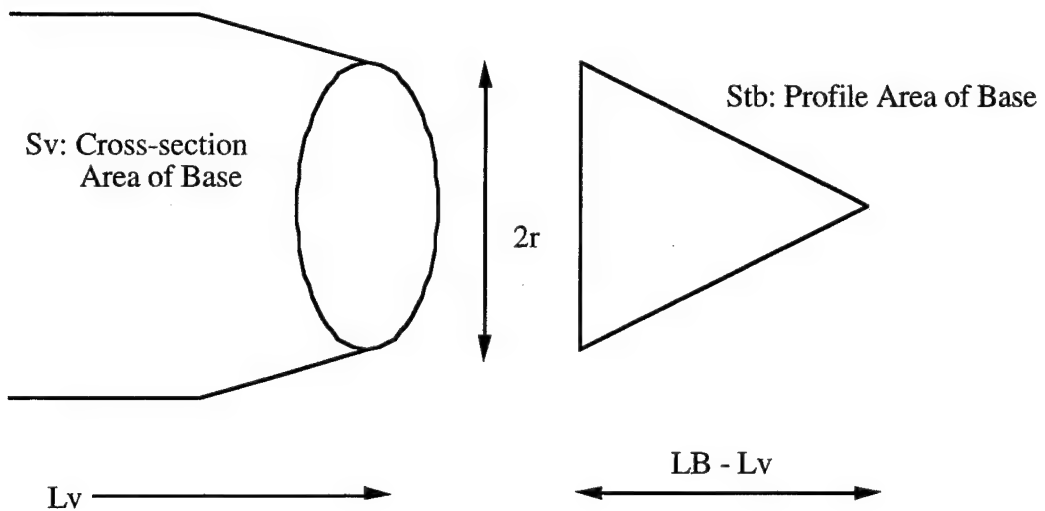


Figure 4. S_v and S_{tb} illustration.

The maximum profile area is determined at the mid-body section where the diameter is maximum.

$$S_b = \frac{\pi d^2}{4} \quad (8)$$

The radius of the body at the axial position L_v is determined by realizing the base profile is a triangle.

$$r = \left(\frac{d}{2} \right) \times \left(1 - \left(\frac{l_v - l_f}{l_b} \right) \right) \quad (9)$$

The cross sectional area at the axial position is therefore

$$S_v = \pi r^2 \quad (10)$$

and the profile area of the base at the axial position is as follows:

$$S_{tb} = r(l_B - l_v) \quad (11)$$

The drag coefficient for the body is initially established by Fidler and Smith [5] and utilized by Wolkerstofer [2]. The value of the drag coefficient will be modified within the parametric study in Chapter III.

$$C_d = 0.29 \quad (12)$$

B. HYDRODYNAMIC COEFFICIENT CALCULATION

From the basic physical description of the system the hydrodynamic parameters can now be determined.

The Lamb's coefficients (k_1 and k_2) of inertia are for a prolate ellipsoid in axial and cross flow. These parameters affect the lift/angle of attack curve slope [3].

$$C_{la} = 2S_v \left(\frac{k_2 - k_1}{S_b} \right) \quad (13)$$

The hydrodynamic coefficient Y_v' is the normal force/angle of attack curve slope [3].

$$Y_{vprime} = \left(\frac{-S_b}{l_B^2} \right) (C_{la} + C_d) \quad (14)$$

The pitching moment/angle of attack curve slope was simplified using MATHCAD and its symbolic manipulator and is based on the cross sectional area of the body of revolution [3].

$$C_{ma} = \frac{2(k_2 - k_1)}{S_b l_B} \times \left[\frac{-\pi d^2 (3x_m - l_n)}{12} + \frac{\pi d^2}{12l_b^2} \times \left(\begin{array}{l} -3x_m l_v^2 + 6l_v x_m l_b + 2l_v^3 - 3l_f l_v^2 - 3l_b l_v^2 \\ + 6x_m l_v l_f - 6x_m l_f l_b + 3l_f^2 l_b - 3x_m l_f^2 + l_f^3 \end{array} \right) \right] \quad (15)$$

The hydrodynamic coefficient N_v' is the pitching moment coefficient [3].

$$N_{vprime} = C_{ma} \times \frac{S_b}{l_B^2} \quad (16)$$

The lift/pitch rate curve slope is a function of the lift/angle of attack curve slope [3].

$$C_{lq} = C_{la} \left(1 - \frac{x_m}{l_B} \right) \quad (17)$$

The rotary derivative hydrodynamic coefficient Y_r' is the normal force/pitch rate coefficient [3].

$$Y_{rprime} = - \frac{C_{lq} S_b}{l_B^2} \quad (18)$$

The pitching moment/pitch rate curve slope [3].

$$C_{mq} = C_{ma} \left[\frac{\left(1 - \frac{x_m}{l_B} \right)^2 - \left(\frac{V(l_{cb} - x_m)}{S_{tb} l_B^2} \right)}{\left(1 - \frac{x_m}{l_B} \right) - \left(\frac{V}{S_{tb} l_B} \right)} \right] \quad (19)$$

The rotary derivative hydrodynamic coefficient N_r' is pitching moment/pitch rate coefficient [3].

$$N_{rprime} = - \frac{C_{mq} S_b}{l_B^2} \quad (20)$$

The acceleration hydrodynamic coefficients Y_V' and N_V' are based on the work of Humphrys and Watkinson [4].

$$Y_{vdotprime} = -\frac{2Vk_2}{l_B^3} \quad (21)$$

$$N_{vdotprime} = -Y_{vdotprime} \quad (22)$$

The rotary acceleration hydrodynamic coefficient is modified by the mass moment of inertia of the displaced fluid about the z axis.

$$I_{zdf} = \int_0^{l_B} \rho S(x) (x_m - x)^2 dx \quad (23)$$

The rotary acceleration hydrodynamic coefficient N_r' is determined from the following relation [4].

$$N_{rdotprime} = -\frac{2k_b I_{zdf}}{\rho l_B^5} \quad (24)$$

C. PROGRAM VALIDATION

We computed the values of the hydrodynamic coefficients using a MATLAB program and utilized the generalizations that will be required for the parametric study. The results were compared to the DATCOM SUBOFF data collected by LT Wolkerstofer [2] and the results are listed in Table 1.

Hydrodynamic Coefficient	DATCOM	Program Function	Percent Error
Y_v'	-0.0058	-0.0058	0
N_v'	-0.0136	-0.0136	0
Y_r'	-0.0014	-0.0014	0
N_r'	-0.0012	-0.0011	8.3
Y_v'	-0.0153	-0.0152	0.6
N_v'	0.0153	0.0152	0.6
N_r'	-0.0007	-0.0007	0

Table 1. DATCOM and program comparison.

The results of the program agree with the data compiled from the actual model tested using the semi-empirical methods. The modifications to simplify the analysis based on the given shapes provided accurate results. The magnitude of the N_r' error is due to the small value of the N_r' coefficient.

III. PARAMETRIC STUDY

A. INTRODUCTION

In conducting a parametric study of the body of revolution, we needed to decide which parameters to vary, which to hold constant and what effects these variations would have on the model. The primary goal was to find non-dimensional parameters that would define the shape sufficiently to accurately predict the hydrodynamic coefficients. The non-dimensional parameters would therefore not be constrained to a given particular size and shape.

The data which completely describes the body of revolution include the sectional lengths and nominal (mid-body) diameter. From this the volume, cross sectional areas, and geometric centers could be calculated and the resulting hydrodynamic coefficients. This initial program was limited to specific non-variable inputs only which produced single case results.

The initial steps in broadening the program were due to non-dimensionalizing the sectional lengths while still specifying the overall length of the body. The diameter was determined from the slenderness ratio. In describing the body in this manner, we determined that the hydrodynamic coefficients were independent of the specific overall length of the body as the bodies parameters were all proportional to the length. We could therefore, alter the sectional fractional values to determine the effects on the hydrodynamic coefficients.

In order to study these variations in a controlled manner we decided to hold the volume of the body as a constant initially. With the volume as a constant, describing the sectional fractional values would determine the remaining parameters. In addition, only the nose and mid-body fractions would be altered since the base fraction would also be defined by default.

From this basis we pursued two approaches, one involving a constant diameter and varying lengths and the second involving a constant length and varying diameter. This vectoral approach was later modified to allow varying lengths utilizing the non-dimensional volume/length³ parameter.

B. PHYSICAL REVIEW OF PARAMETER MODIFICATIONS

In order to appreciate the multitude of possible parameter modifications Figures 5 through 8 are presented to solidify the physical changes incorporated in the parametric study. Figure 5 is the basic shape of the body of revolution. We have repeated this shape behind the modified shapes for Figures 6 through 8.

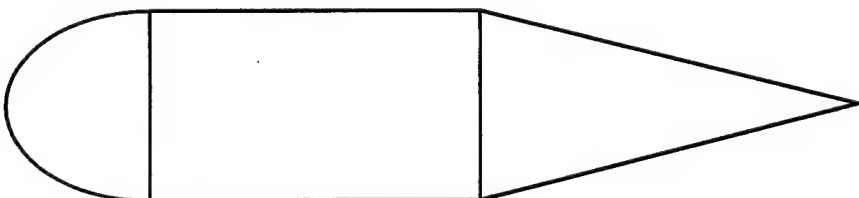


Figure 5. Basic shape.

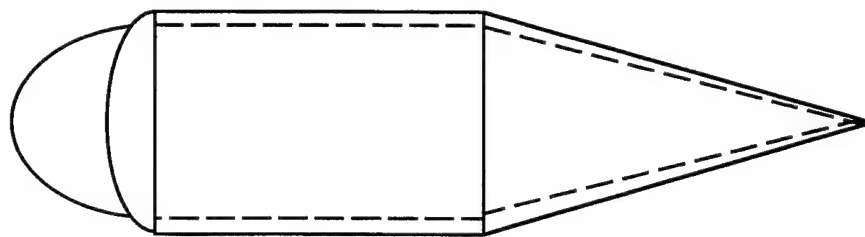


Figure 6. Lower F_n and slenderness ratio (shorter and fatter).

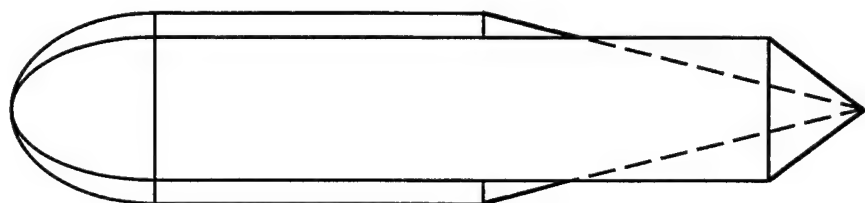


Figure 7. Higher F_m and lower F_b , higher slenderness ratio(slimmer).

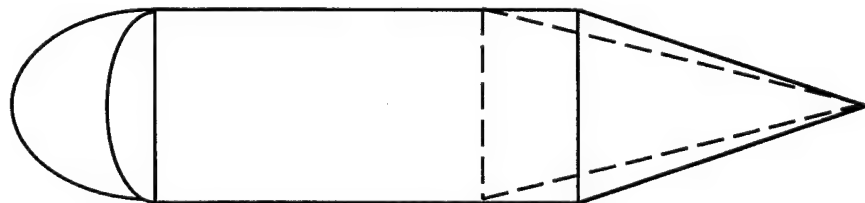


Figure 8. Lower F_n , higher F_m , lower F_b , constant slenderness ratio.

C. COMPUTER MODEL DEVELOPMENT

In the process of the parametric study, the geometry of the body would be altered which would affect the assumptions and variables of the semi-empirical method utilized. The primary concern was with the drag coefficient. The changed shape will induce a different drag. We researched the significance and

magnitude of these modifications on the hydrodynamic coefficients. The value of drag coefficient was a constant 0.29 for various nose and base configurations in Fidler and Smith [5] but at the extreme sectional fractions it must be modified. We utilized the values from Herner [6] in the extreme cases. When the nose length to diameter ratio was less than 1 the coefficient of drag was smoothly increased to the maximum value of 0.82. When the base length to diameter ratio was less than 1 the coefficient of drag was smoothly increased to the maximum value of 0.64. When incorporated into the program this parameter variation had minimal effect on the final result since the other components prescribed by the parameter values dominated the solution trend and our specific area of interest is not at the sectional fractional extreme.

The data format illustrated in Figure 9 demonstrates the limits of the model and is useful in interpreting the mesh graphs.

Since the nose, mid-body and base fractions together comprise 100% of the body the values in the lower right hand side diagonal are not possible combinations and an arbitrary constant value is utilized to complete the matrix and provide a visible floor to the mesh graphs. Appendix A is the MATLAB program that generated the matrix data with the full range of nose and mid-body fractons.

Mid-Body Fraction

↓

Nose Fraction

	0	10	20	30	40	50	60	70	80	90	100
0	100	90	80	70	60	50	40	30	20	10	0
10	90	80	70	60	50	40	30	20	10	0	
20	80	70	60	50	40	30	20	10	0		
30	70	60	50	40	30	20	10	0			
40	60	50	40	30	20	10	0				
50	50	40	30	20	10	0					
60	40	30	20	10	0						
70	30	20	10	0							
80	20	10	0								
90	10	0									
100	0										

Matrix Body: Base Fraction

Figure 9. Matrix interpretation for data analysis.

D. HYDRODYNAMIC COEFFICIENT MESH GRAPHS

The Figures 10 through 17 were generated with an automatic scaling feature. This allows for a rough comparison of the magnitude of each parameter to be compared to another parameter. The Y_V' variations are significant while the acceleration hydrodynamic coefficients variations in magnitude are relatively small. The graphs of N_V' and N_r' included a clipping feature to allow for the three dimensional viewing. The clipping only involves truncating the values after the solution begins to reach an extreme value.

The Figures 19 through 32 are scaled to determine the shape of the hydrodynamic coefficient and its variations over the entire range of sectional fractions. Each hydrodynamic coefficient mesh graph is

coupled with a two dimensional graph which is not clipped and illustrates the varying parameter in a simpler and therefore more clean environment.

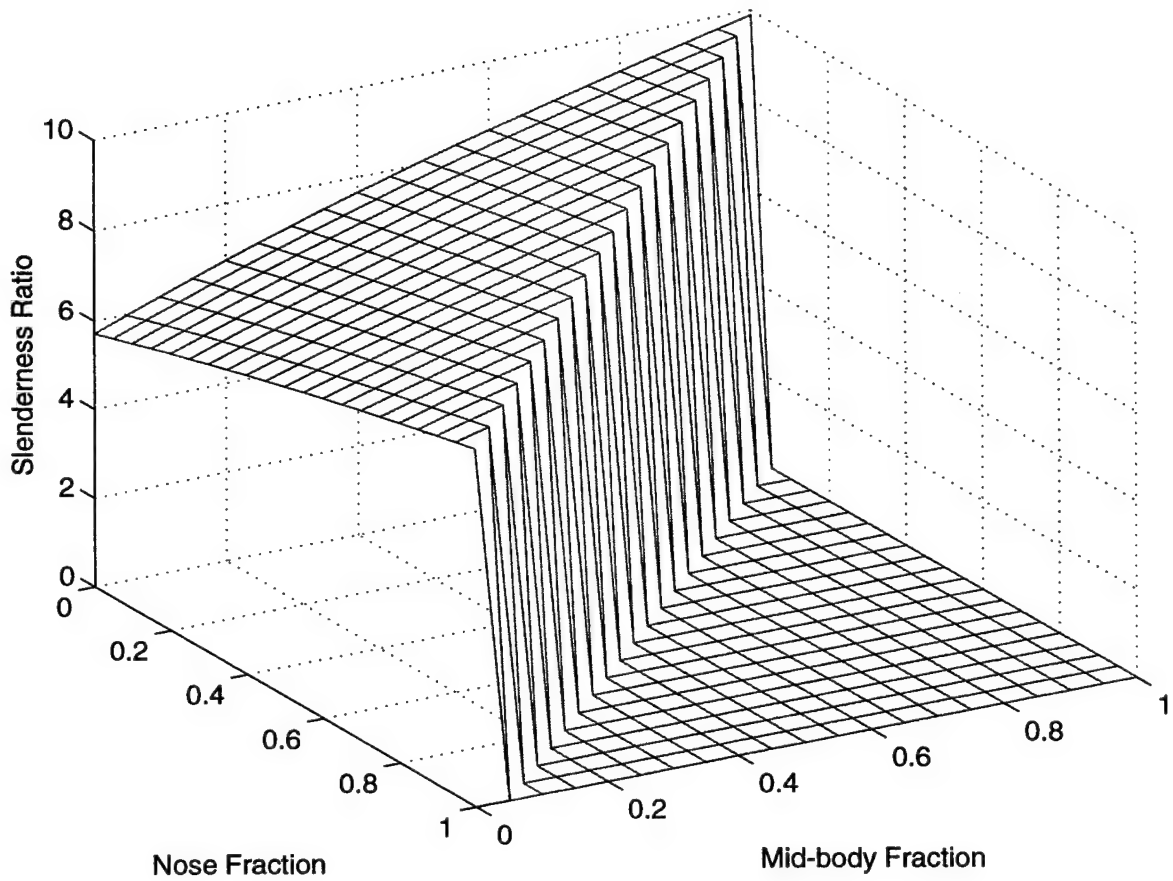


Figure 10. Slenderness ratio mesh graph.

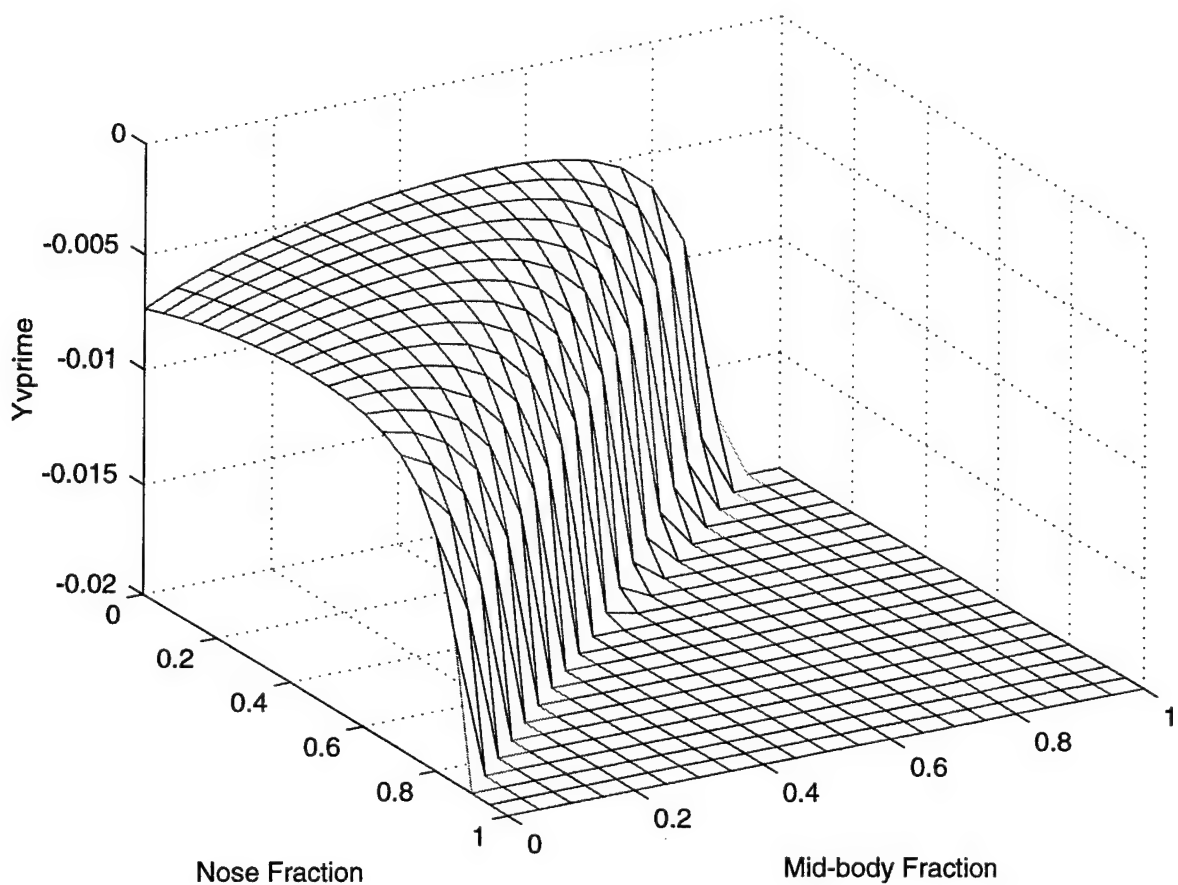


Figure 11. Y_{vprime} standard scale mesh graph.

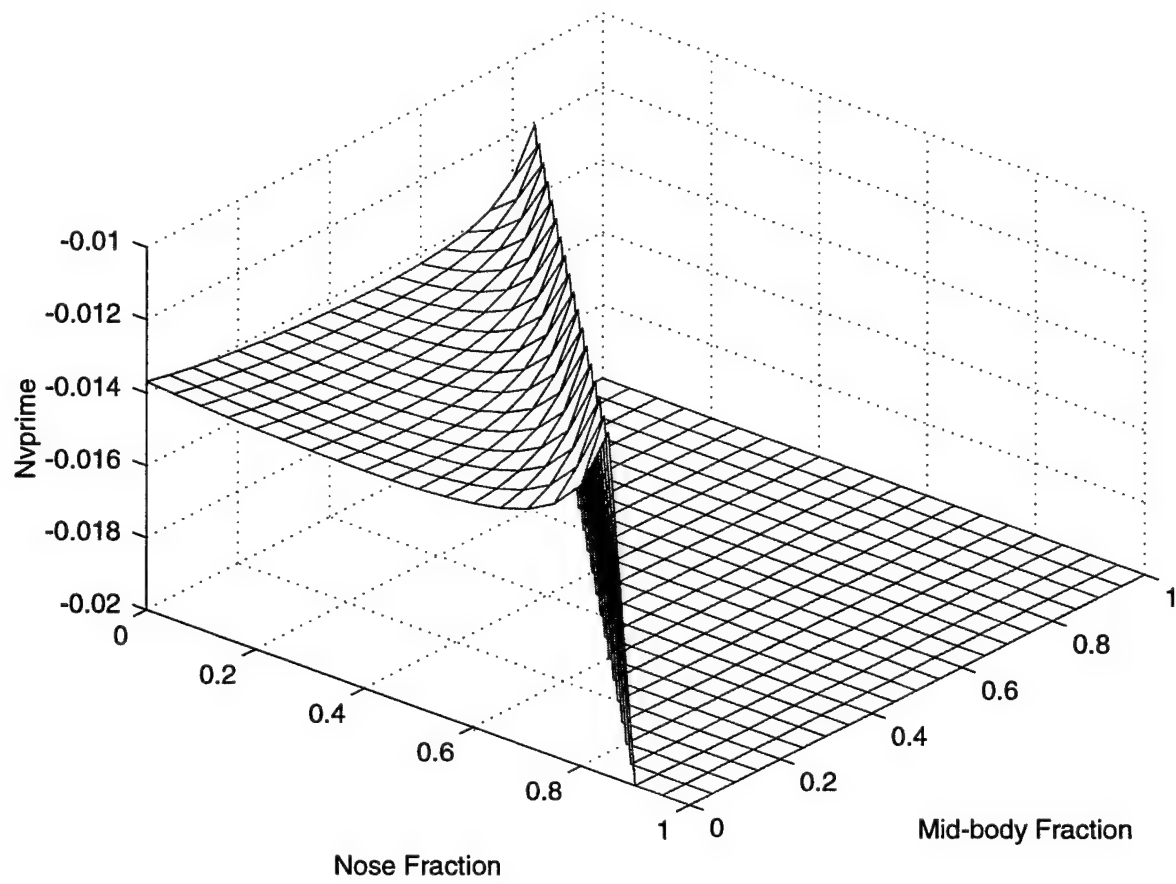


Figure 12. N_{vprime} standard scale mesh graph.

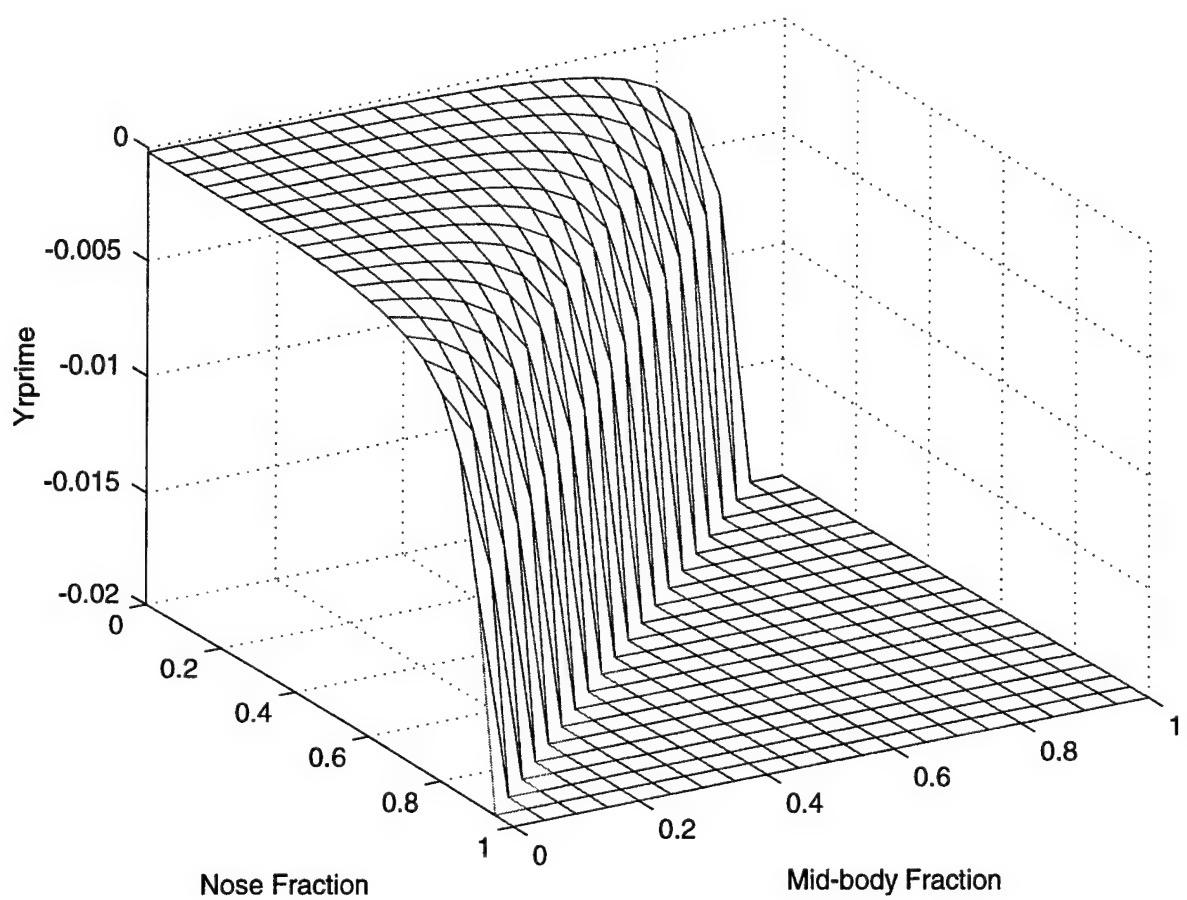


Figure 13. Y_{rprime} standard scale mesh graph.

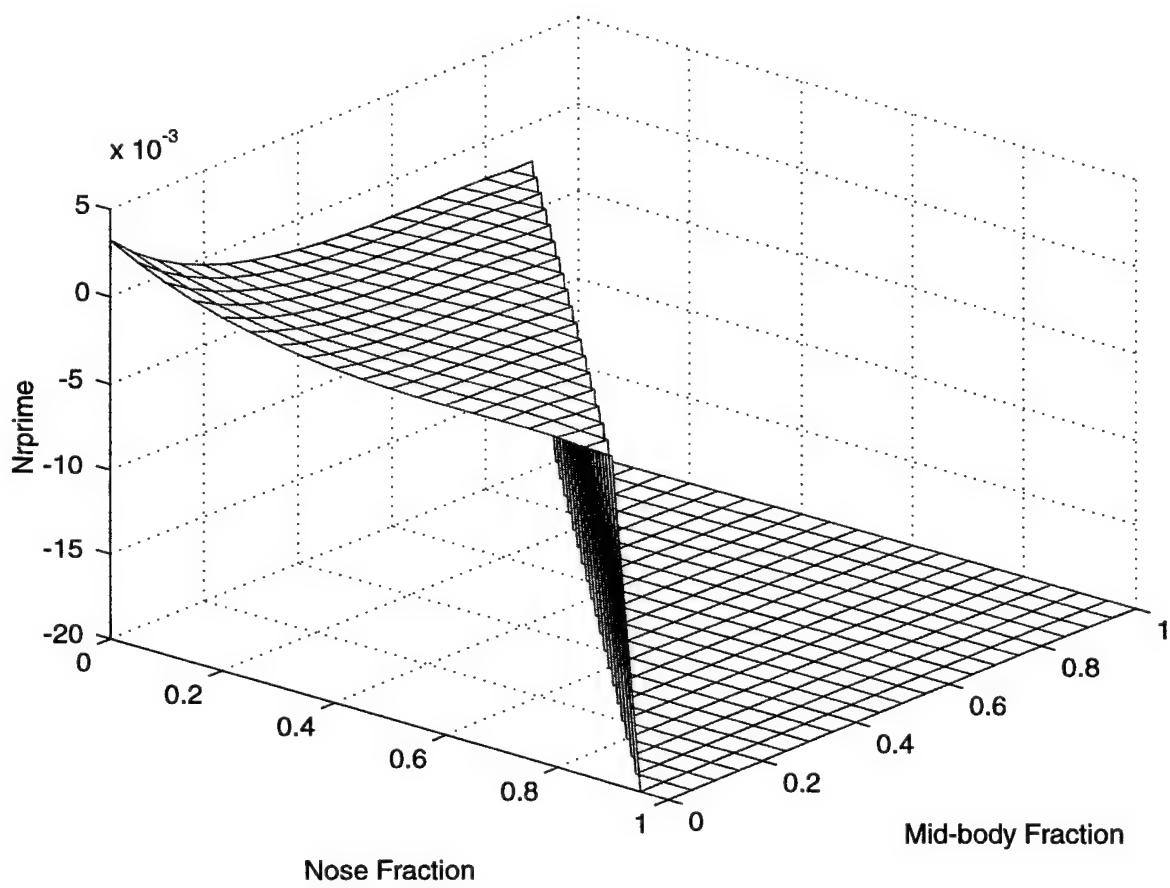


Figure 14. $Nrprime$ standard scale mesh graph.

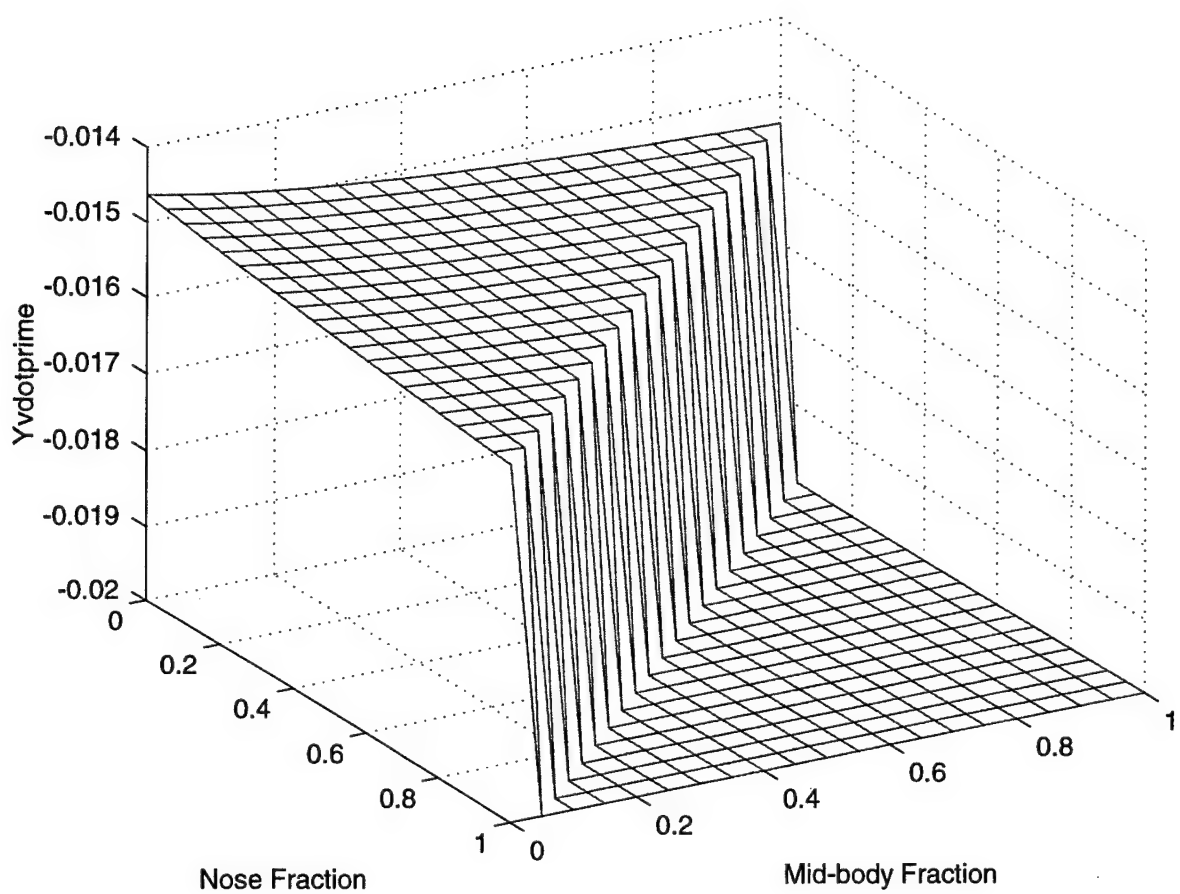


Figure 15. $Y_{vdprime}$ standard scale mesh graph.

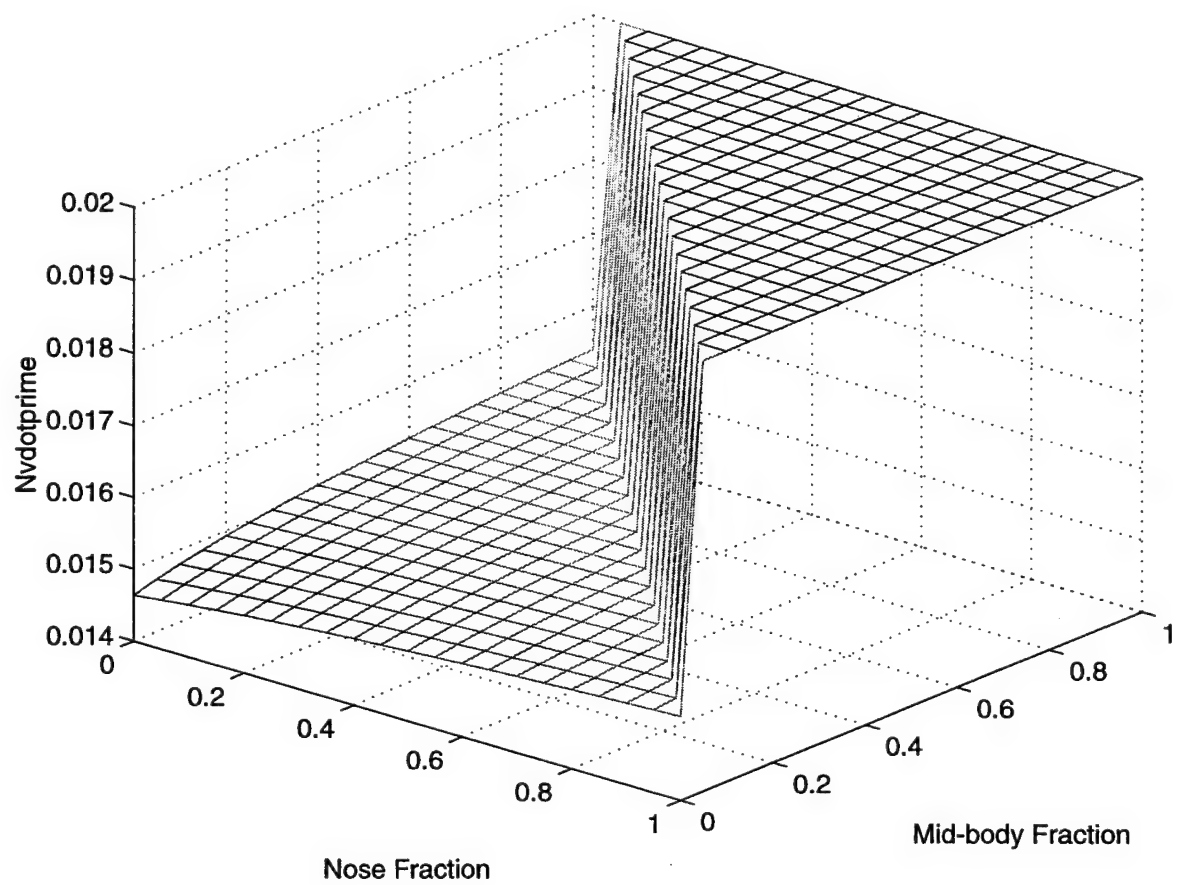


Figure 16. $Nvdprime$ standard scale mesh graph.

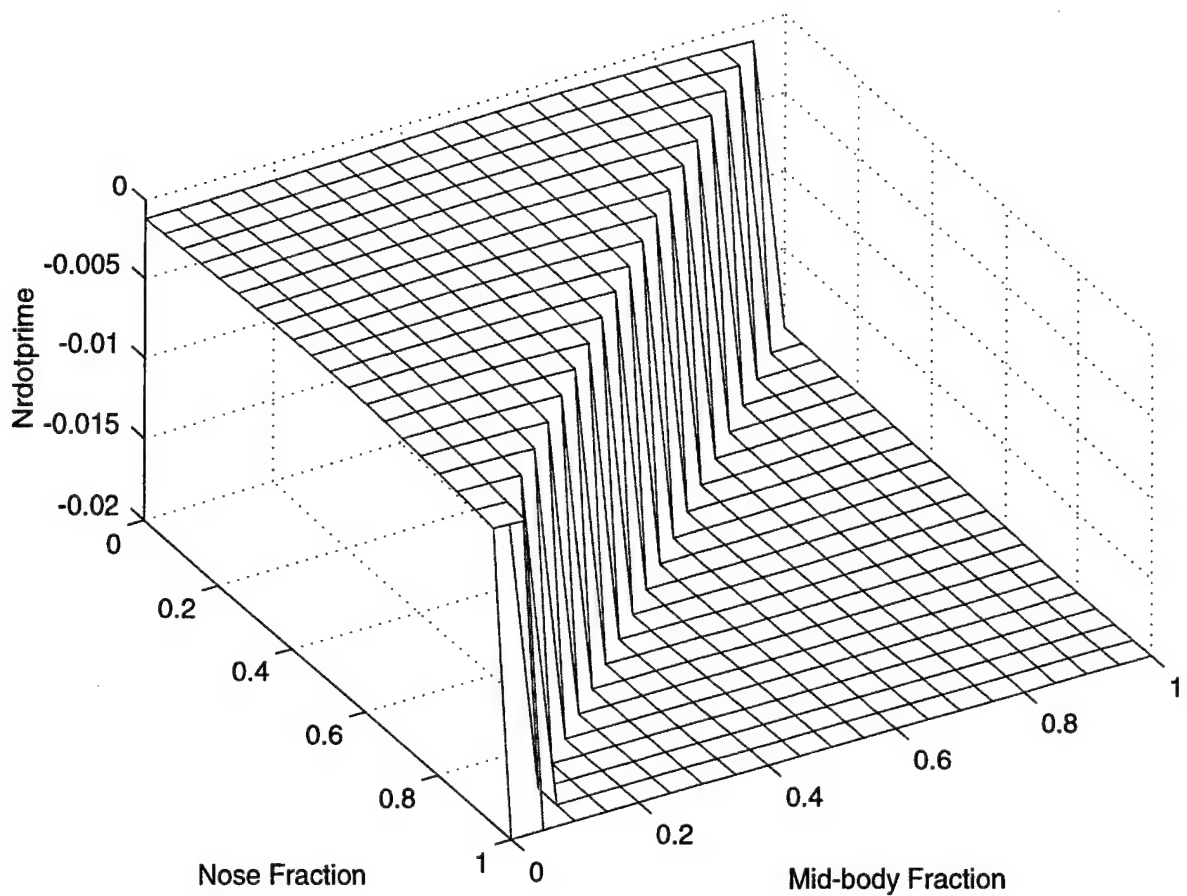


Figure 17. $Nrdprime$ standard scale mesh graph.

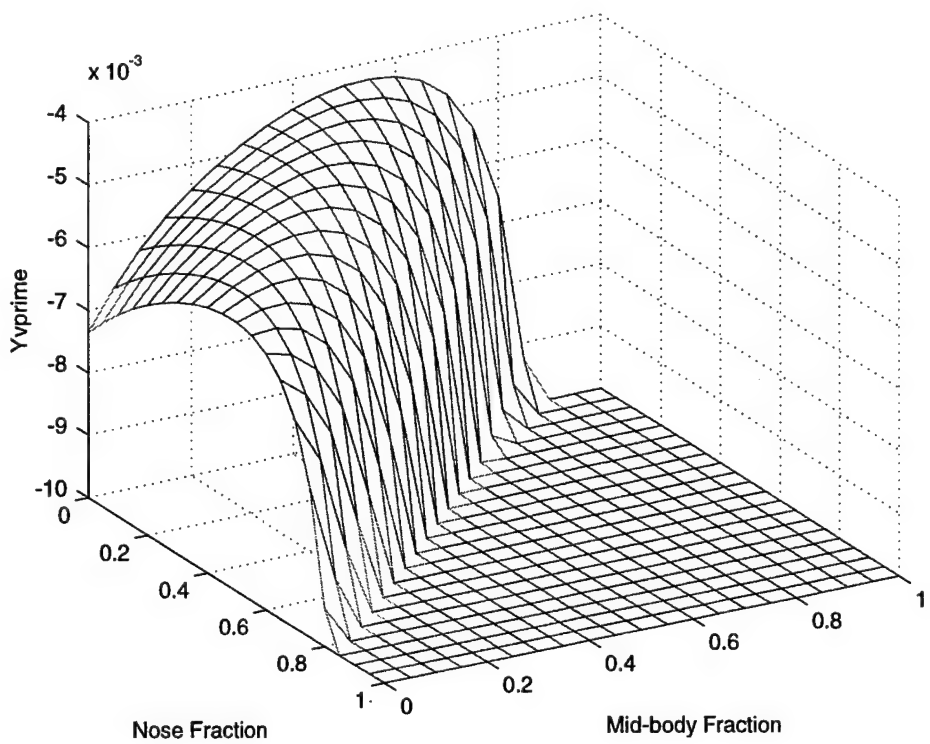


Figure 18. $Yvprime$ close-up scale mesh graph.

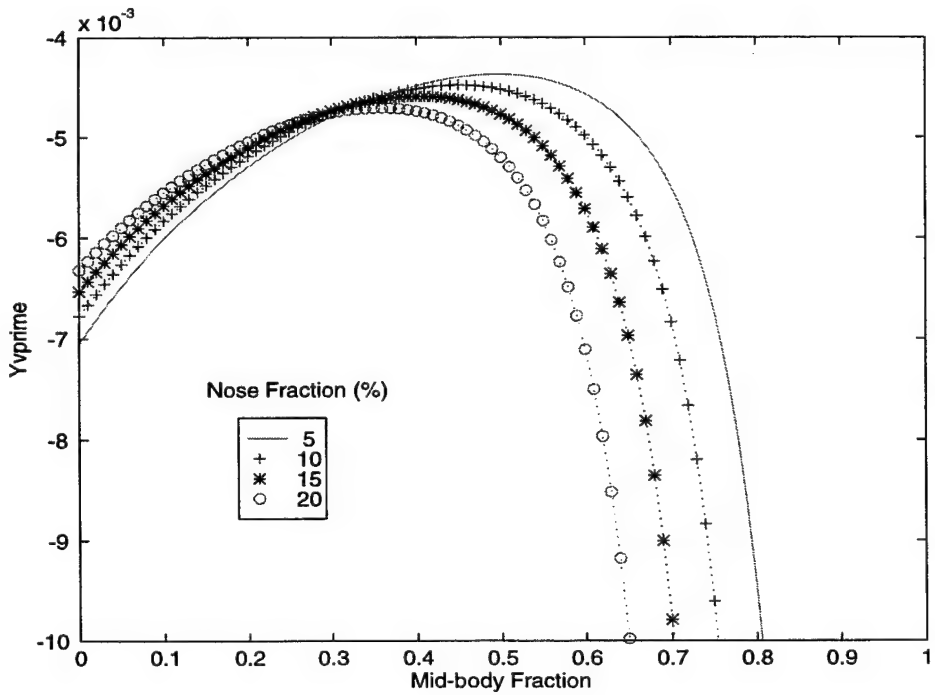


Figure 19. $Yvprime$ variations with mid-body fraction.

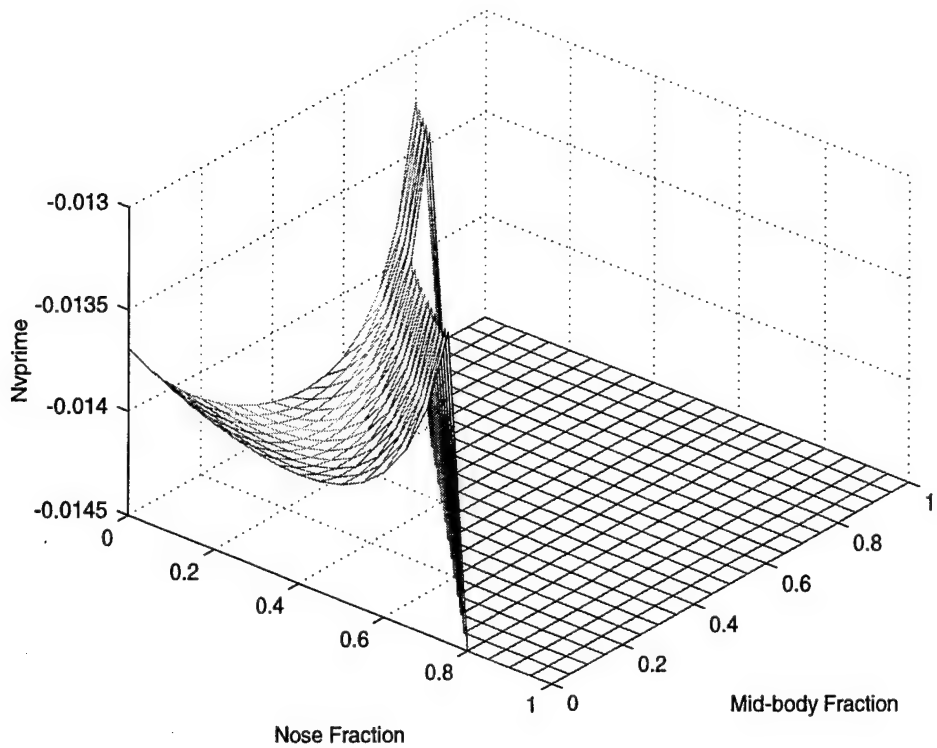


Figure 20. N_{vprime} close-up scale mesh graph.

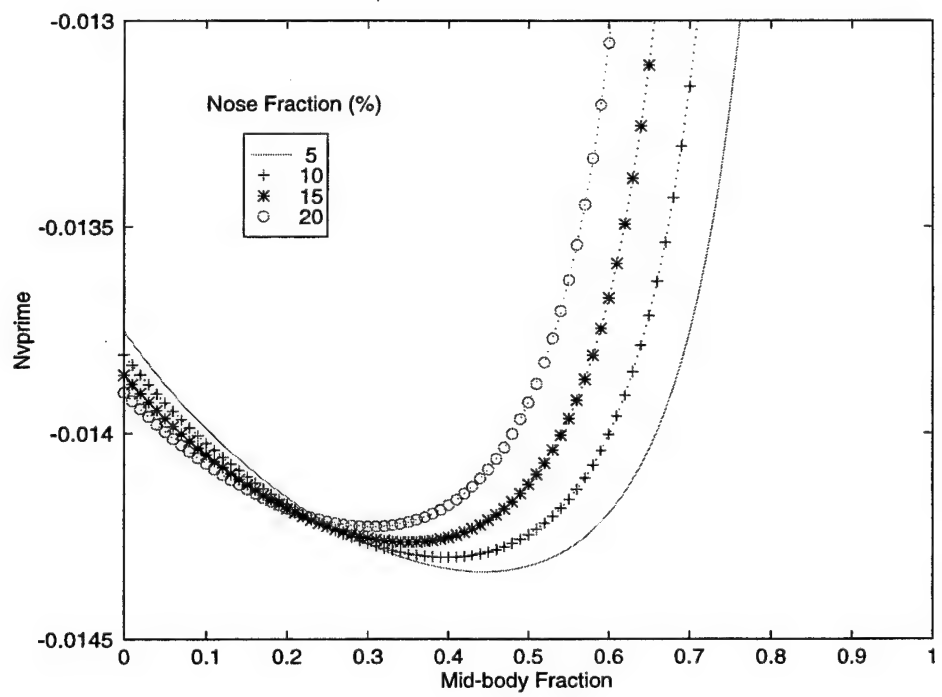


Figure 21. N_{vprime} variations with mid-body fraction.

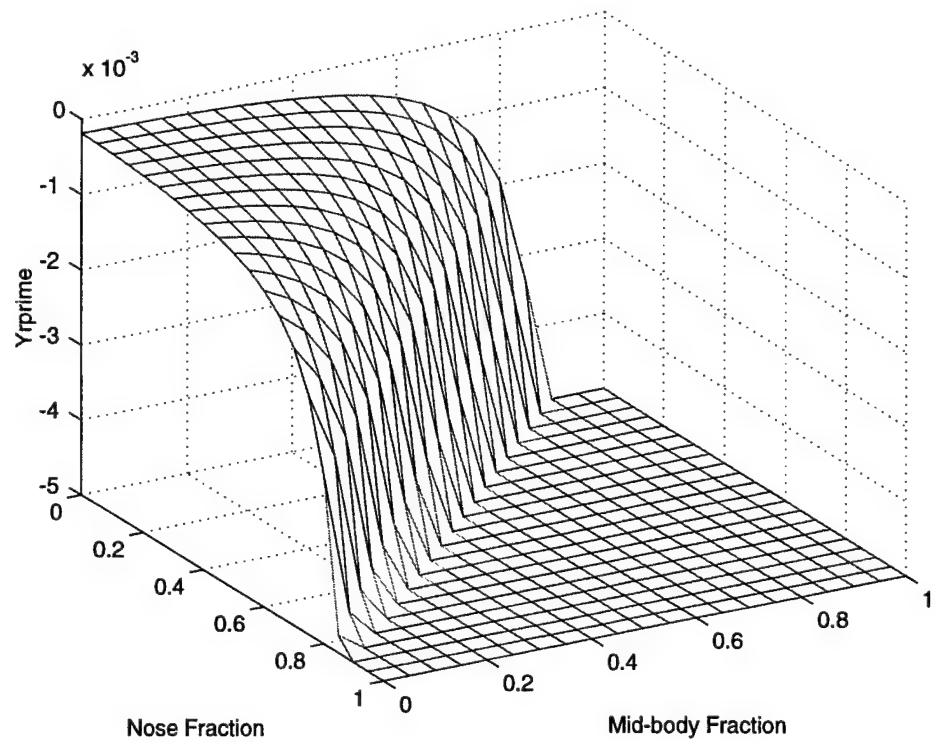


Figure 22. Y_{rprime} close-up scale mesh graph.

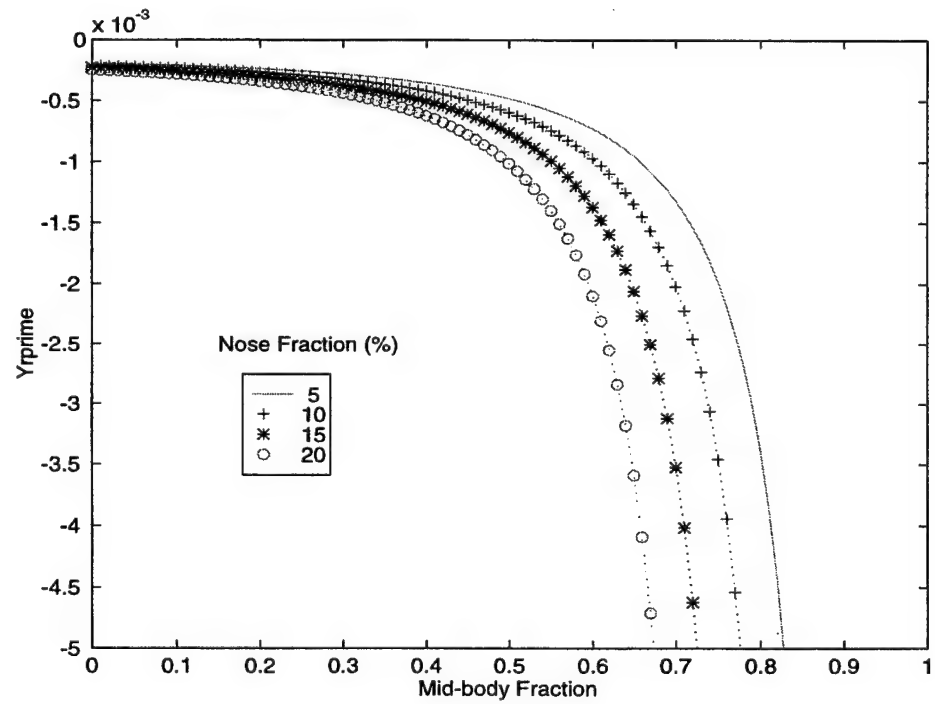


Figure 23. Y_{rprime} variations with mid-body fraction.

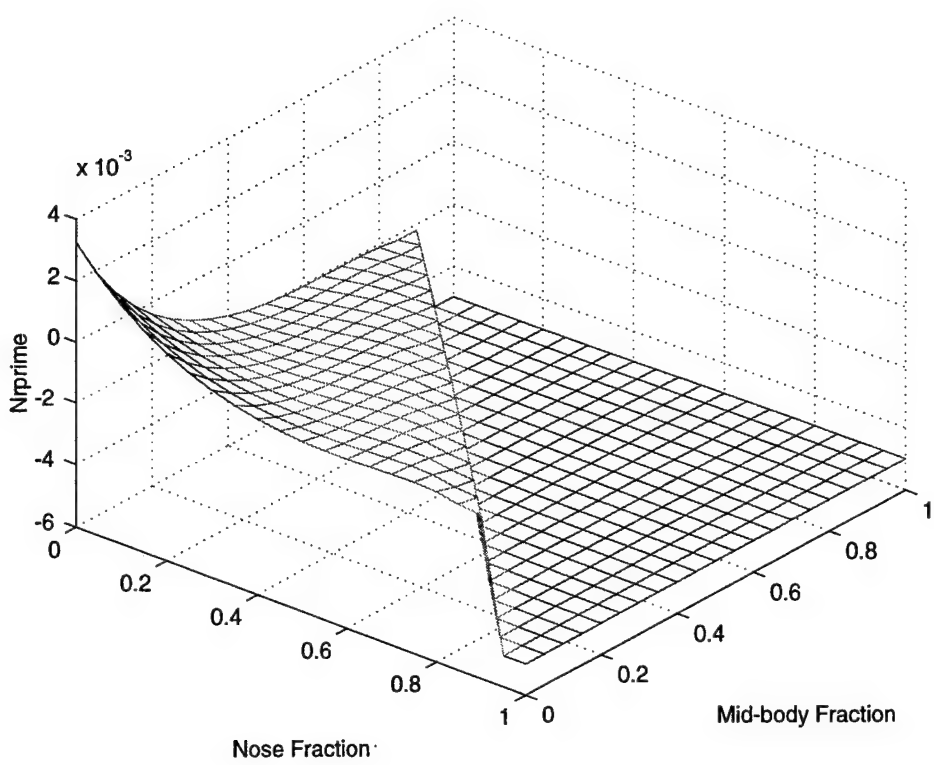


Figure 24. $Nrprime$ close-up scale mesh graph.

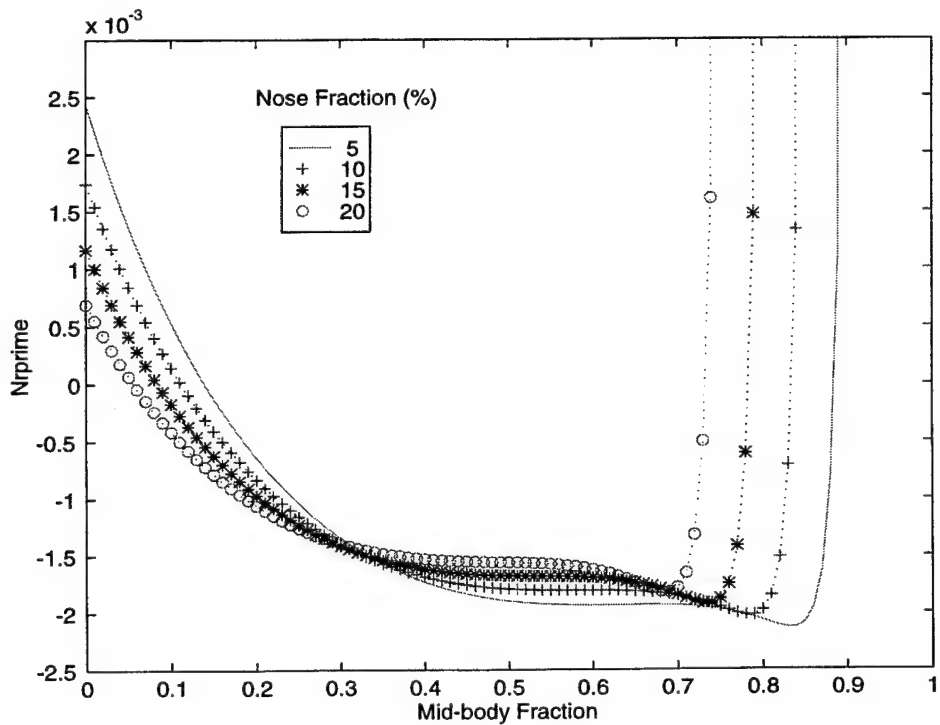


Figure 25. $Nrprime$ variations with mid-body fraction.

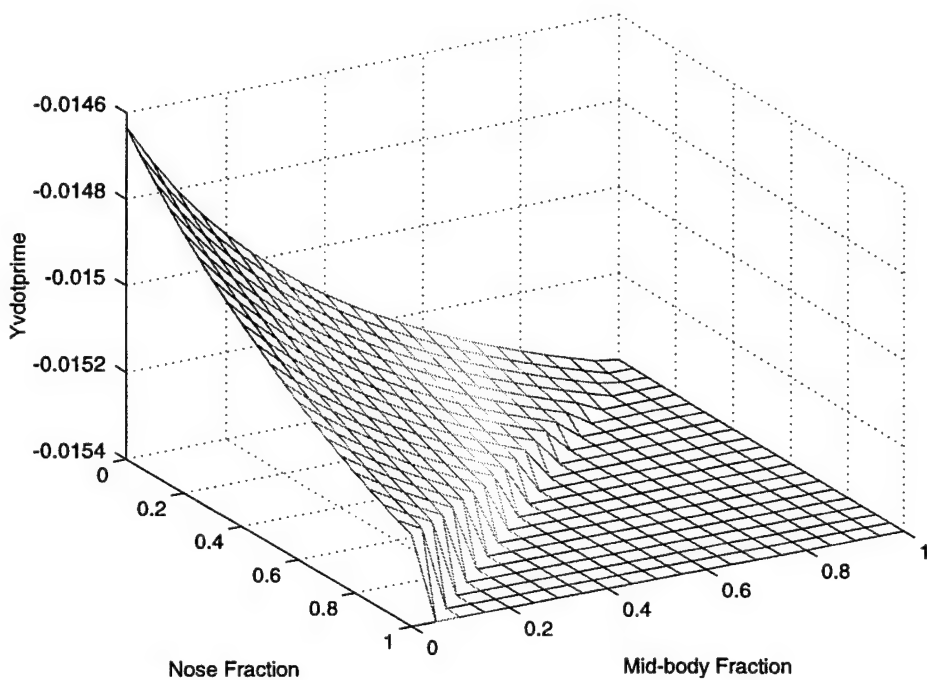


Figure 26. $Yvdprime$ close-up scale mesh graph.

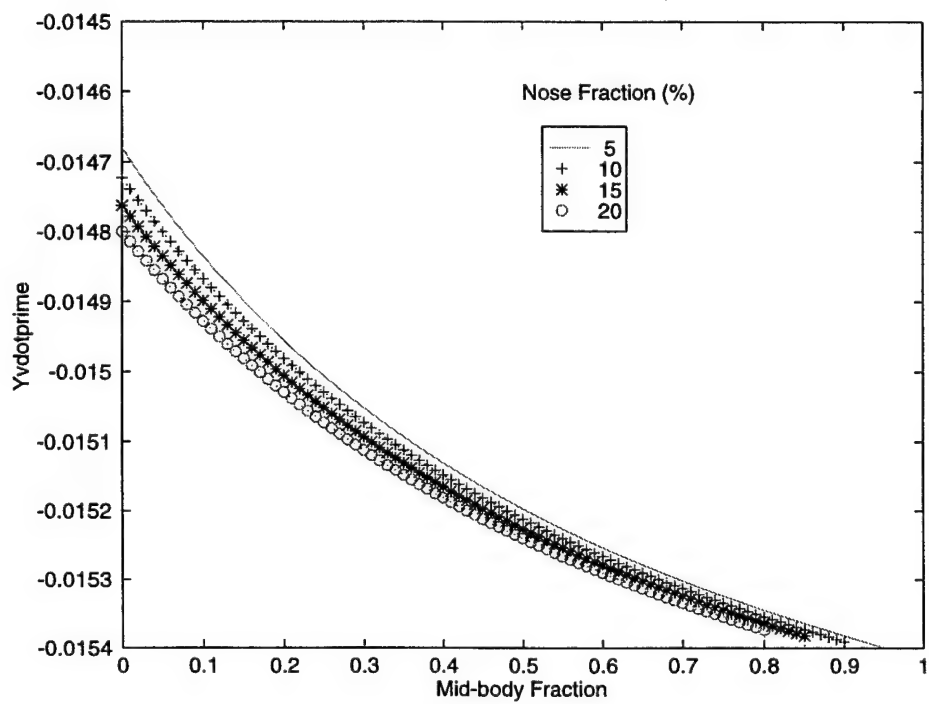


Figure 27. $Yvdprime$ variations with mid-body fraction.

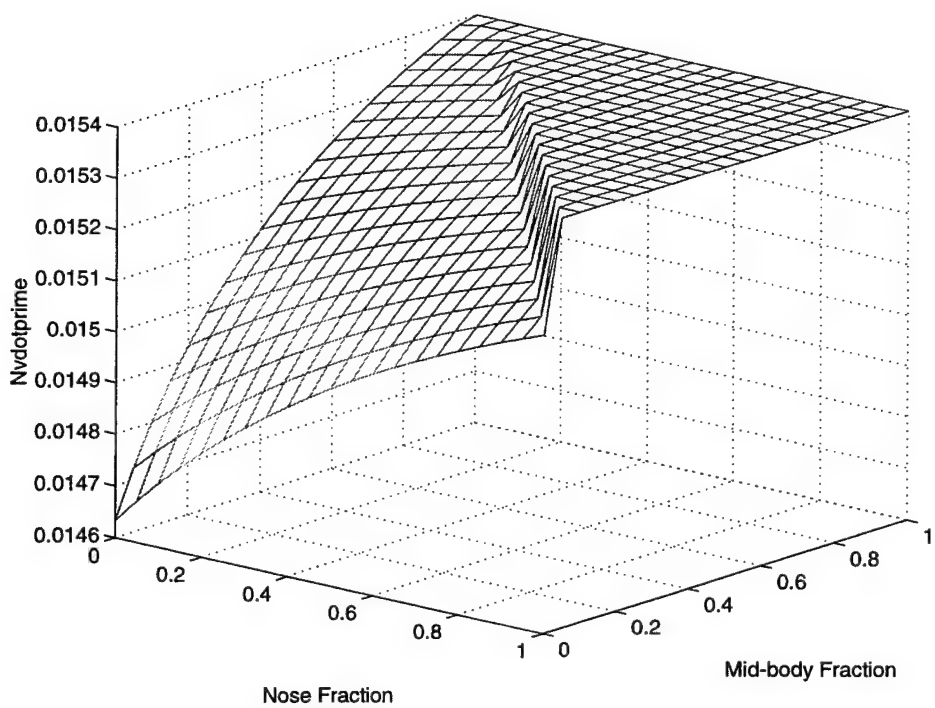


Figure 28. $Nvdprime$ close-up scale mesh graph.

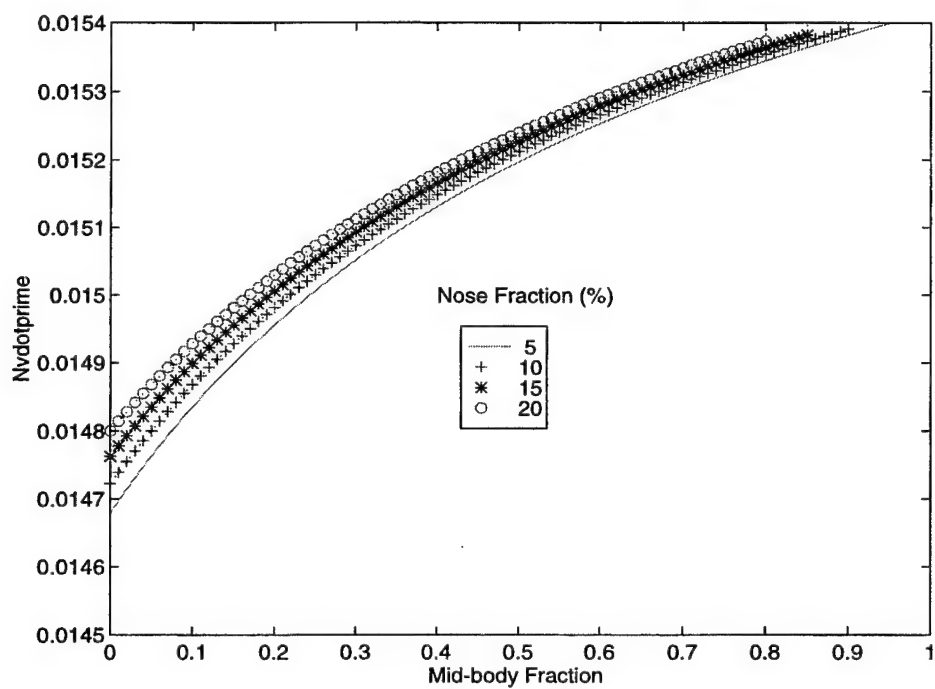


Figure 29. $Nvdprime$ variations with mid-body fraction.

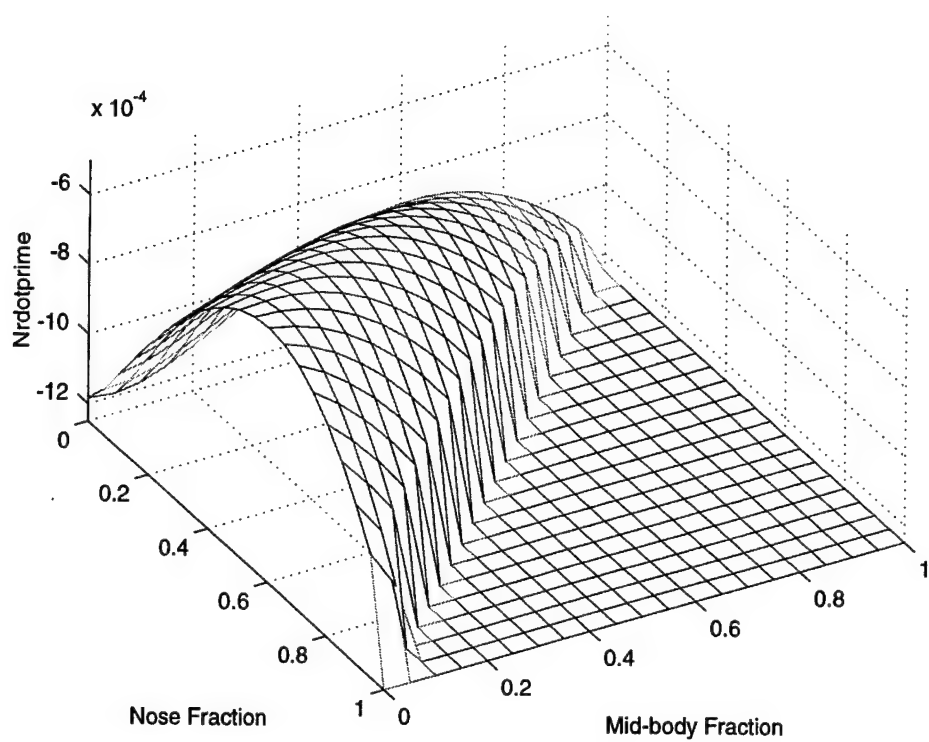


Figure 30. Nrdprime close-up scale mesh graph.

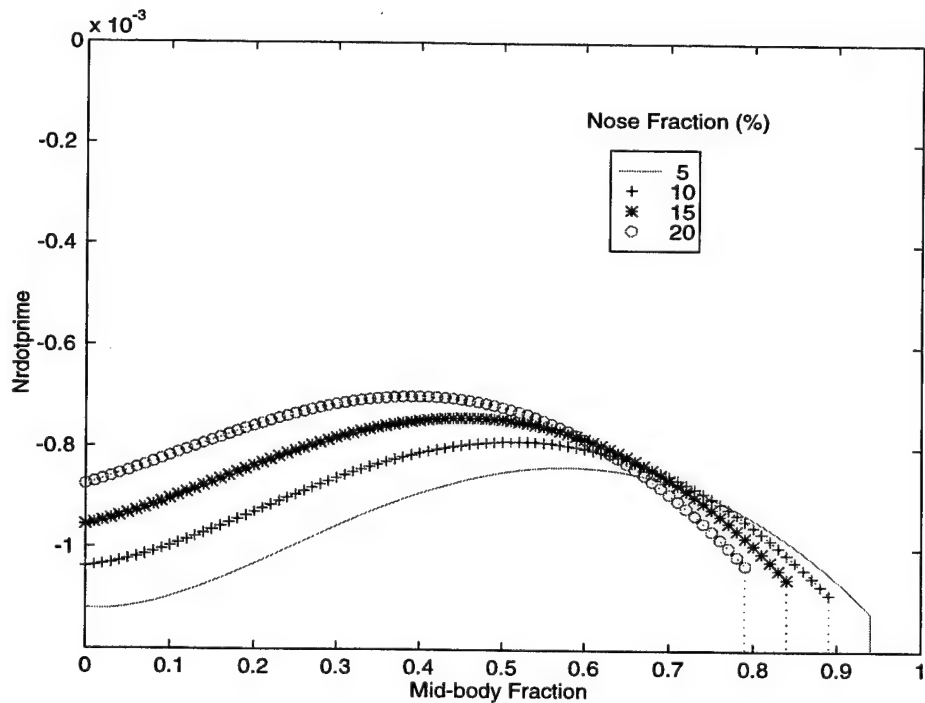


Figure 31. Nrdprime variations with mid-body fraction.

E. VOLUME AND LENGTH VARIATIONS

The mesh graphs of the hydrodynamic coefficients were generated holding the volume of the body of revolution constant. We now explored variations in the volume and length parameters of the body of revolution to see the effects on the hydrodynamic coefficients as illustrated in Figure 32.

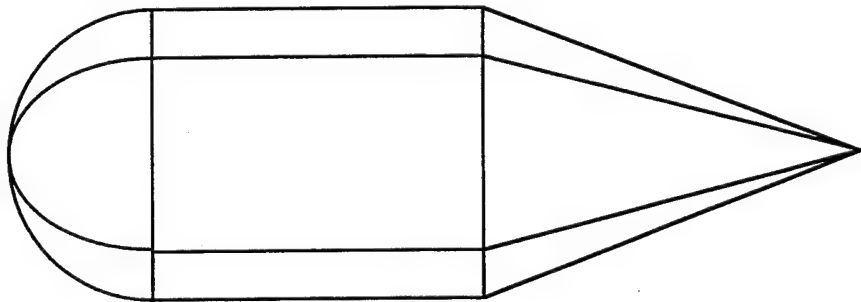


Figure 32. Variations of V/L^3 ratio drawing.

We took the basic body and coupled the volume and length to determine if a non-dimensional volume/length³ ratio was valid. The non-dimensional results matched the original results. The value of volume/length³ for the body was 8.023×10^{-3} . With this value as an average value we varied the volume/length³ ratio from 6 to 10×10^{-3} . The range is noted on all figures as 6 to 10 for simplicity. The smaller value is due to a smaller volume or a larger overall length. Figures 33 through 46 investigate these variations at nose fractions of 10% and 20%. For the vast majority of the entire range variations of volume/length³ result in linear trends in all cases.

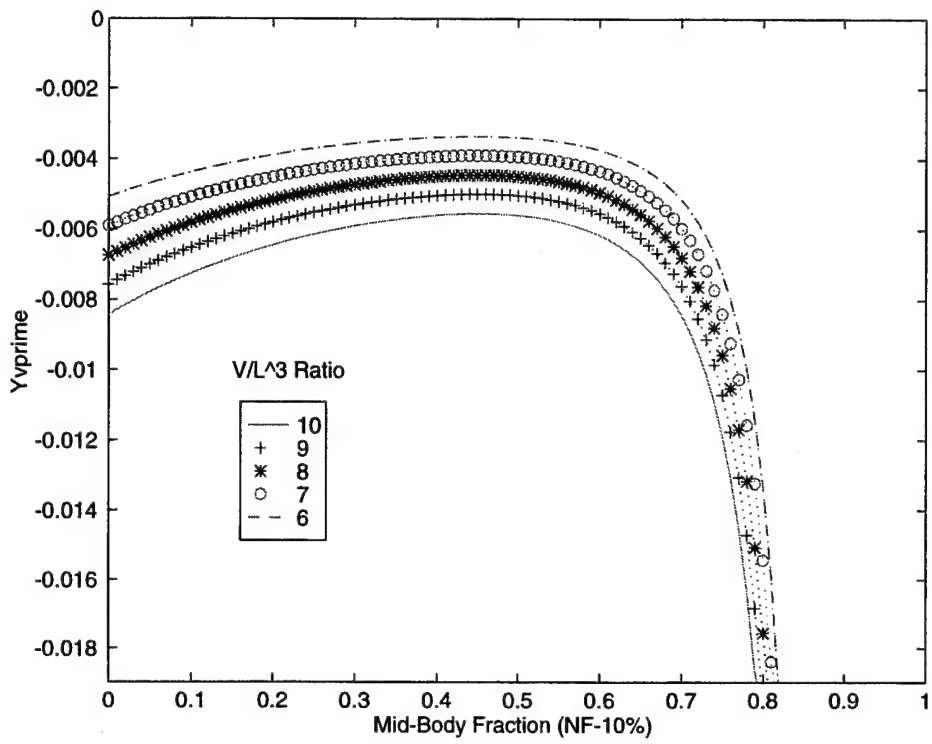


Figure 33. Y'_{vprime} V/L^3 variations at 10% nose fraction.

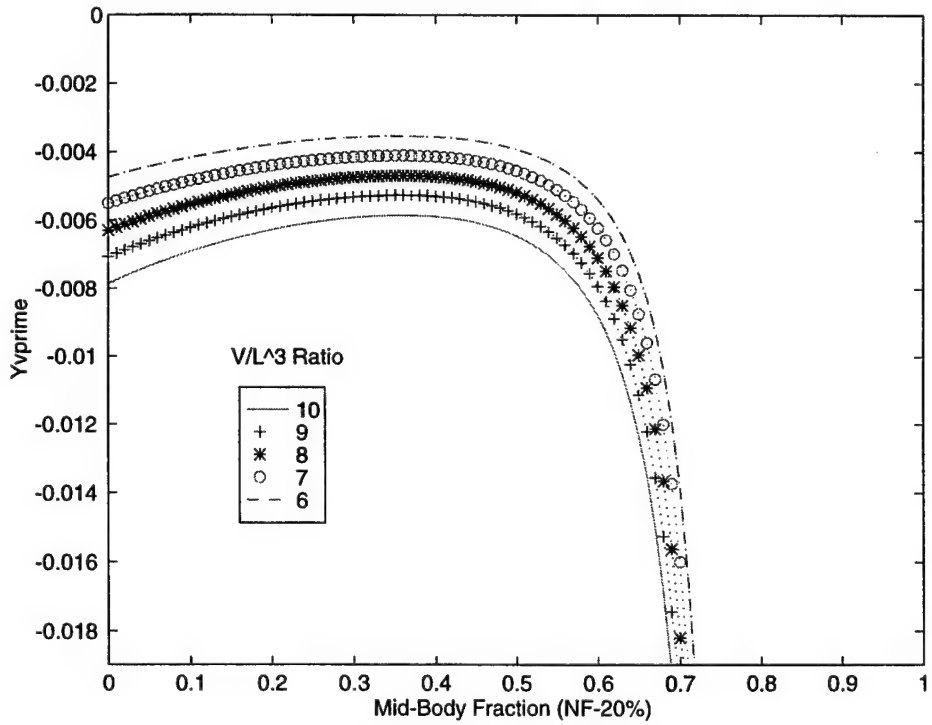


Figure 34. Y'_{vprime} V/L^3 variations at 20% nose fraction.

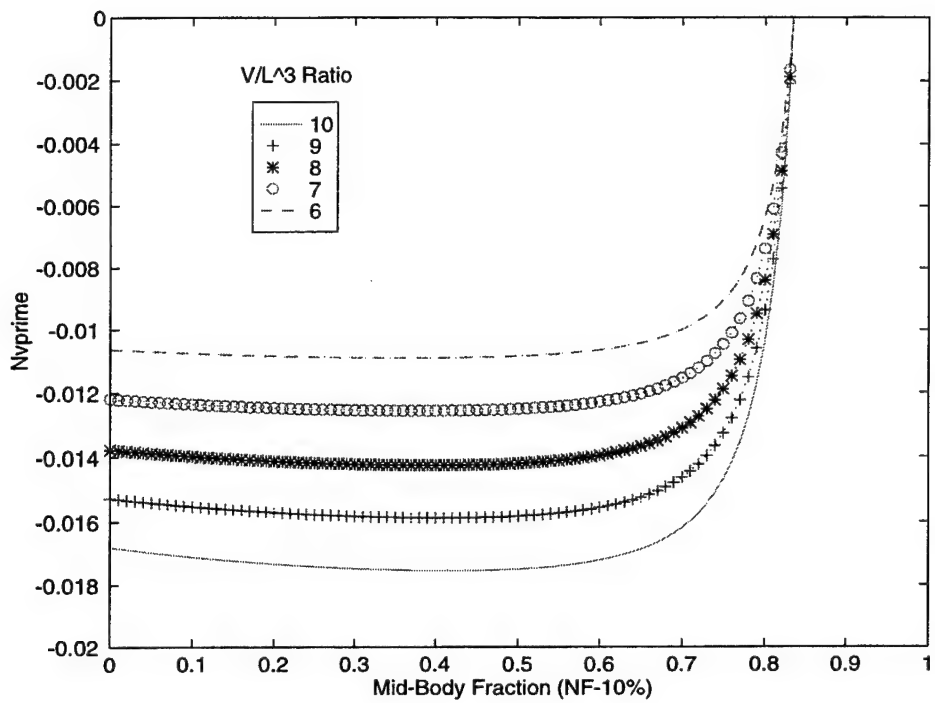


Figure 35. N_{vprime} V/L^3 variations at 10% nose fraction.

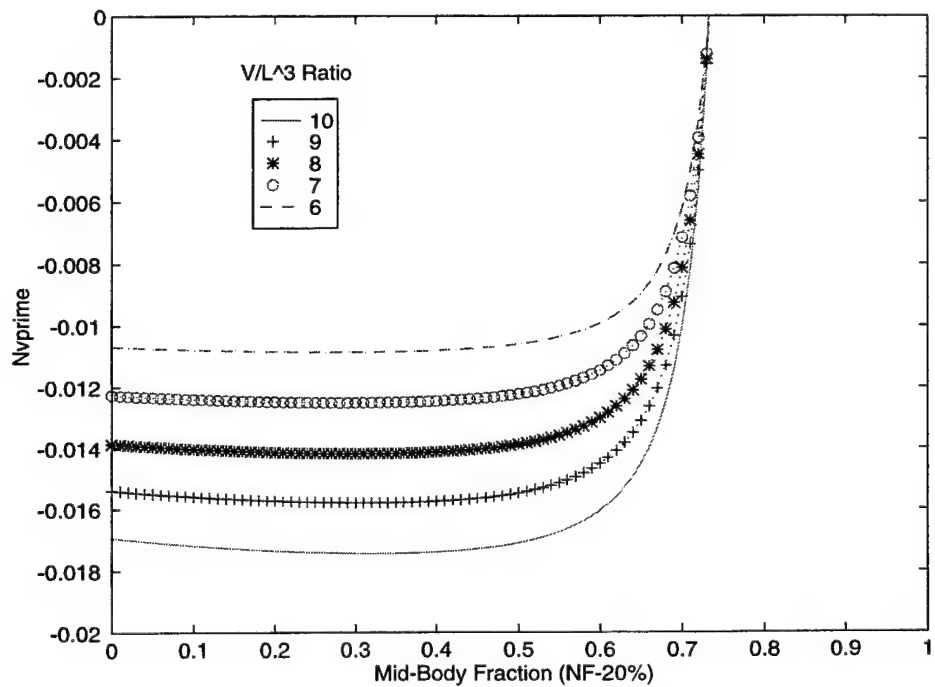


Figure 36. N_{vprime} V/L^3 variations at 20% nose fraction.

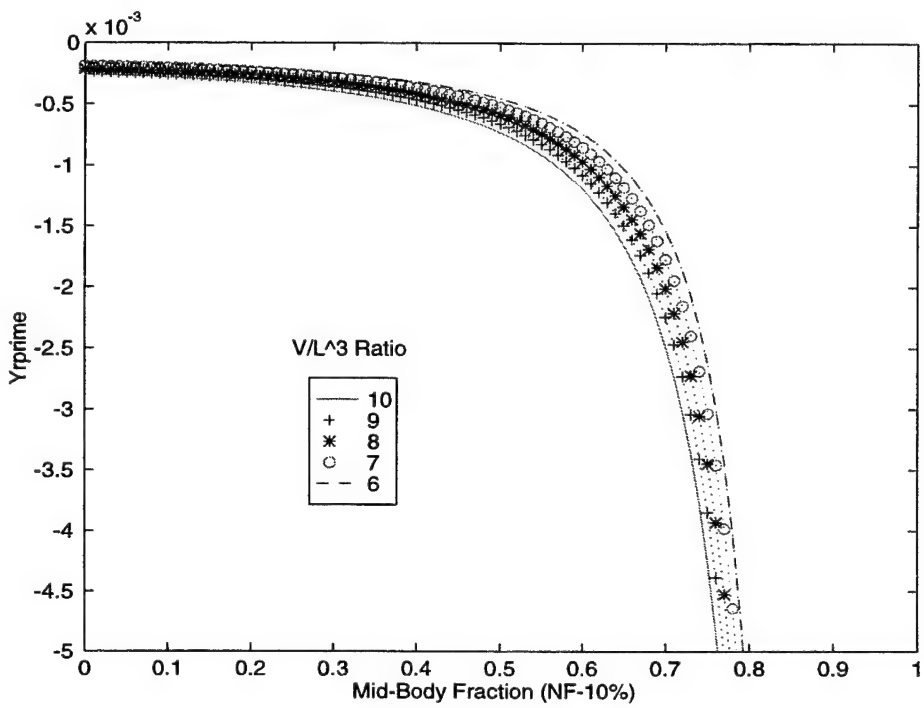


Figure 37. Y_{rprime} V/L^3 variations at 10% nose fraction.

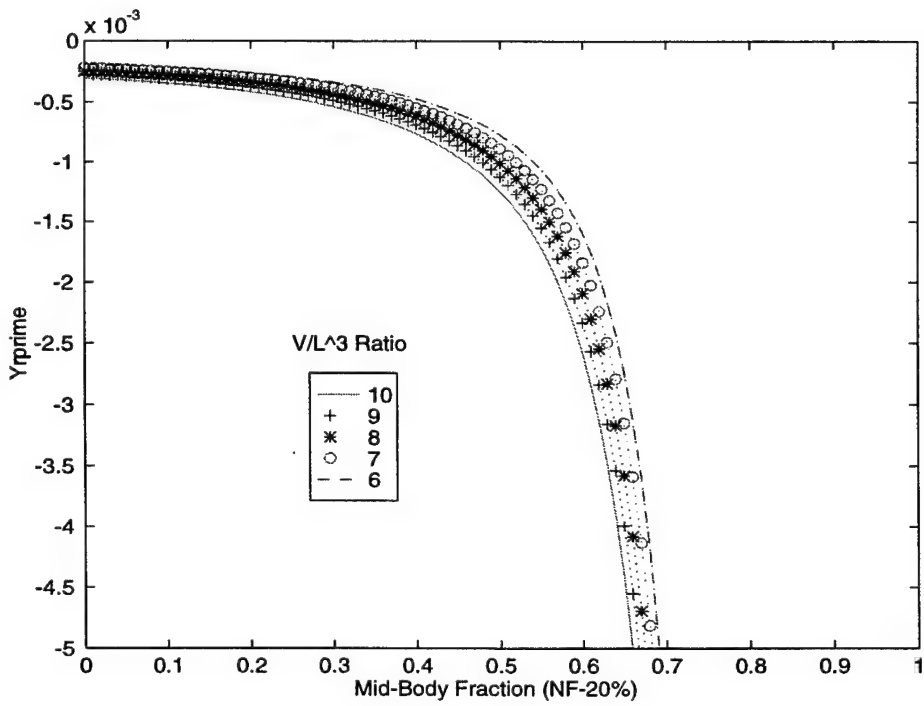


Figure 38. Y_{rprime} V/L^3 variations at 20% nose fraction.

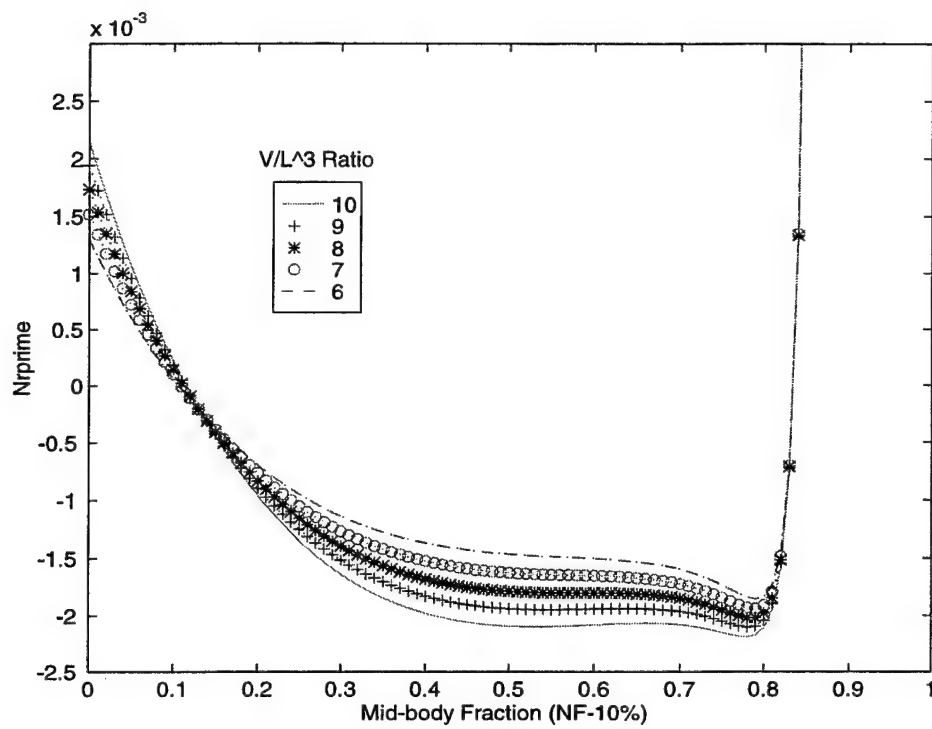


Figure 39. $Nrprime V/L^3$ variations at 10% nose fraction.

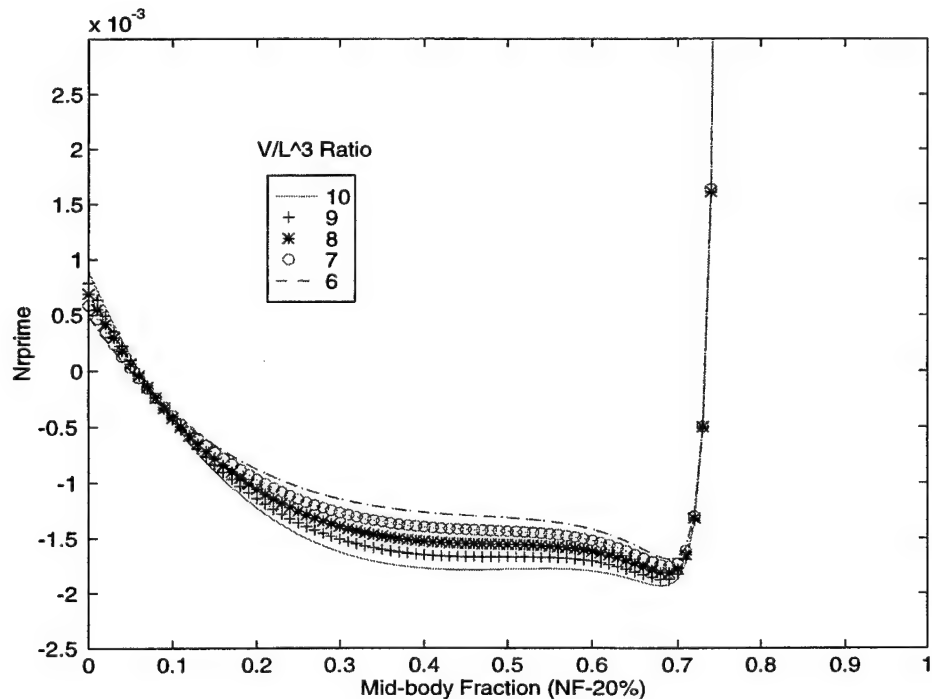


Figure 40. $Nrprime V/L^3$ variations at 20% nose fraction.

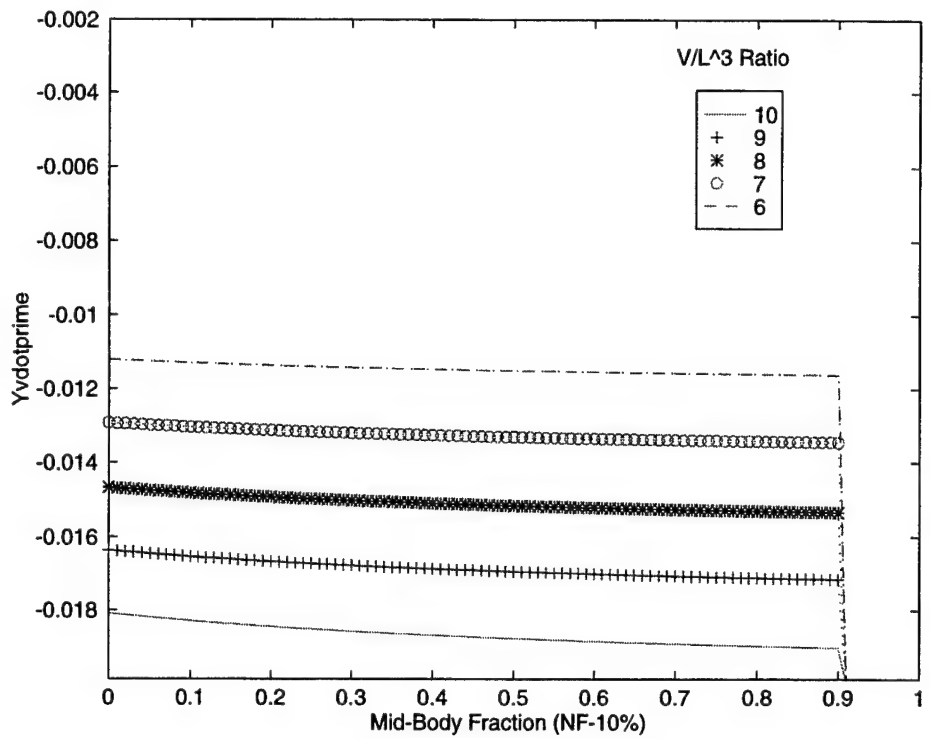


Figure 41. $Y_{vdprime}$ V/L^3 variations at 10% nose fraction.

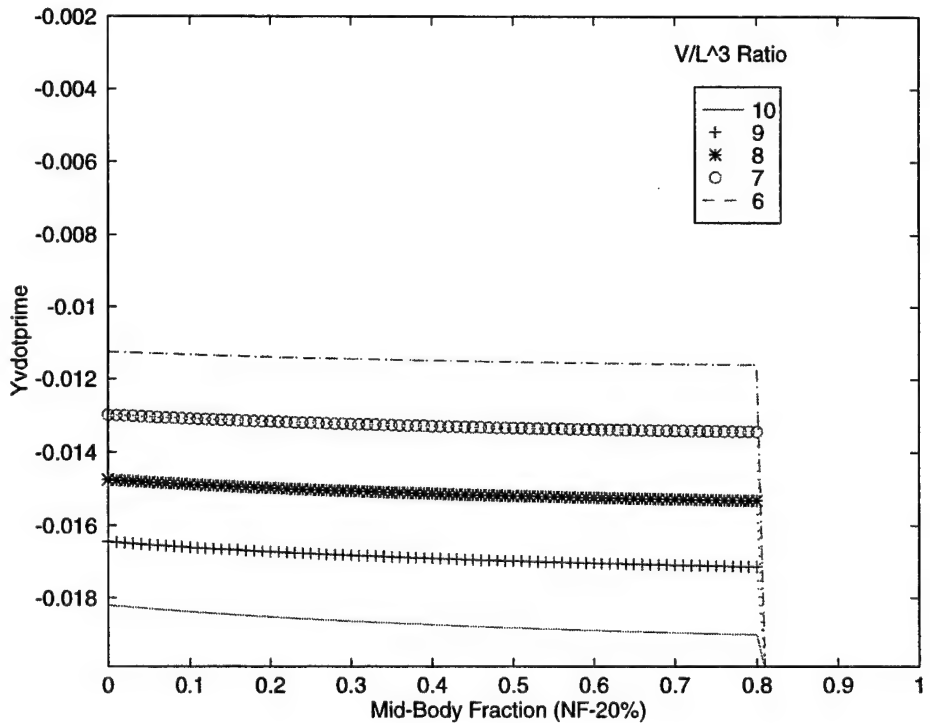


Figure 42. $Y_{vdprime}$ V/L^3 variations at 20% nose fraction.

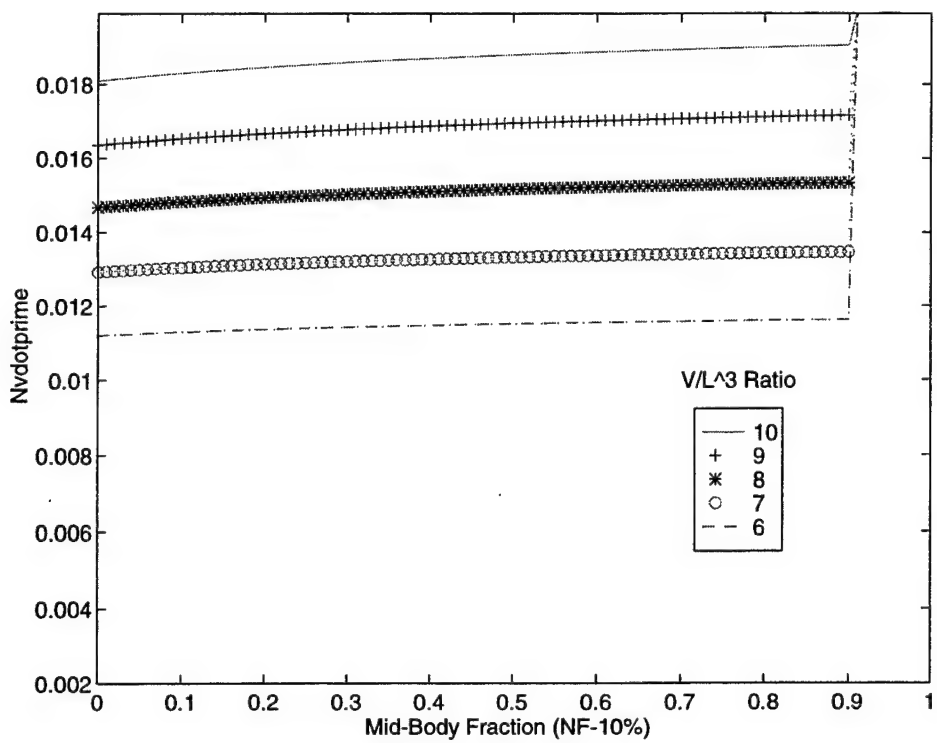


Figure 43. Nvdprime V/L^3 variations at 10% nose fraction.

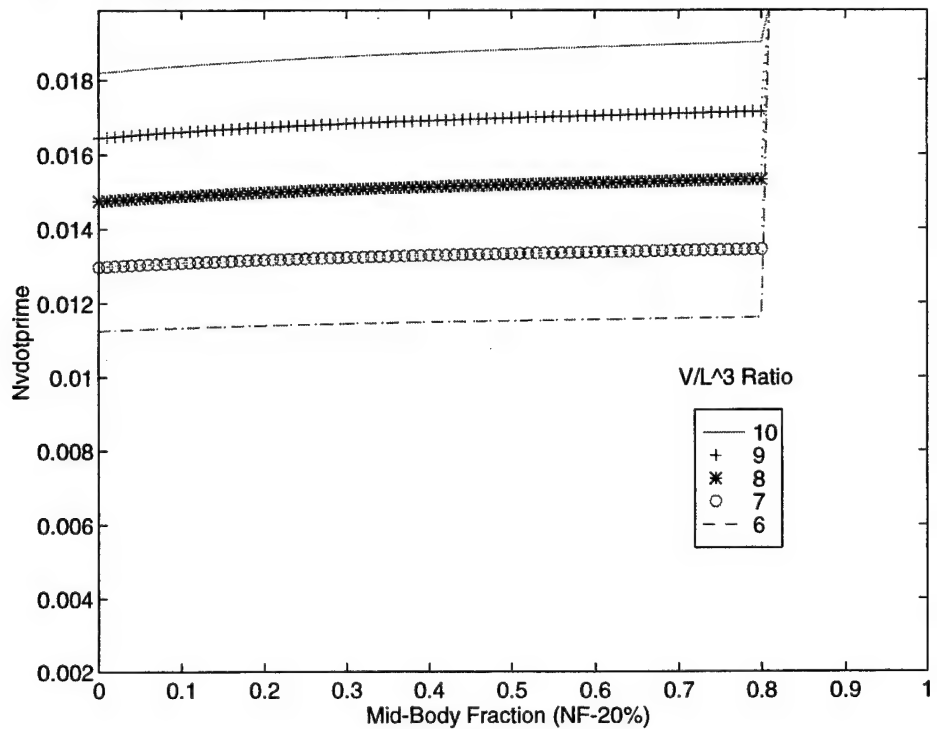


Figure 44. Nvdprime V/L^3 variations at 20% nose fraction.

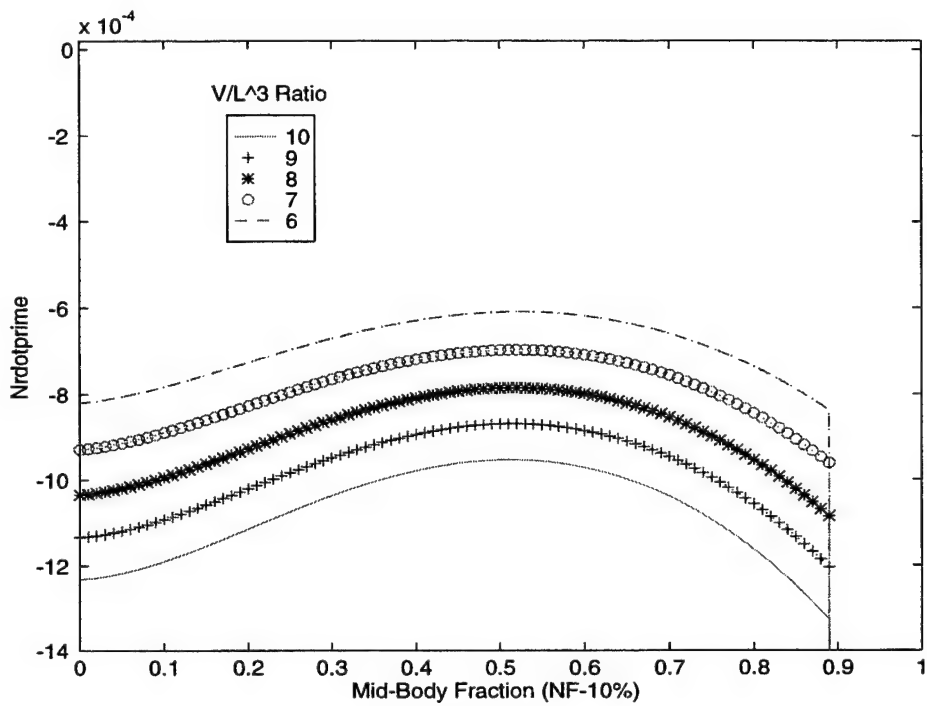


Figure 45. Nrdprime V/L^3 variations at 10% nose fraction.

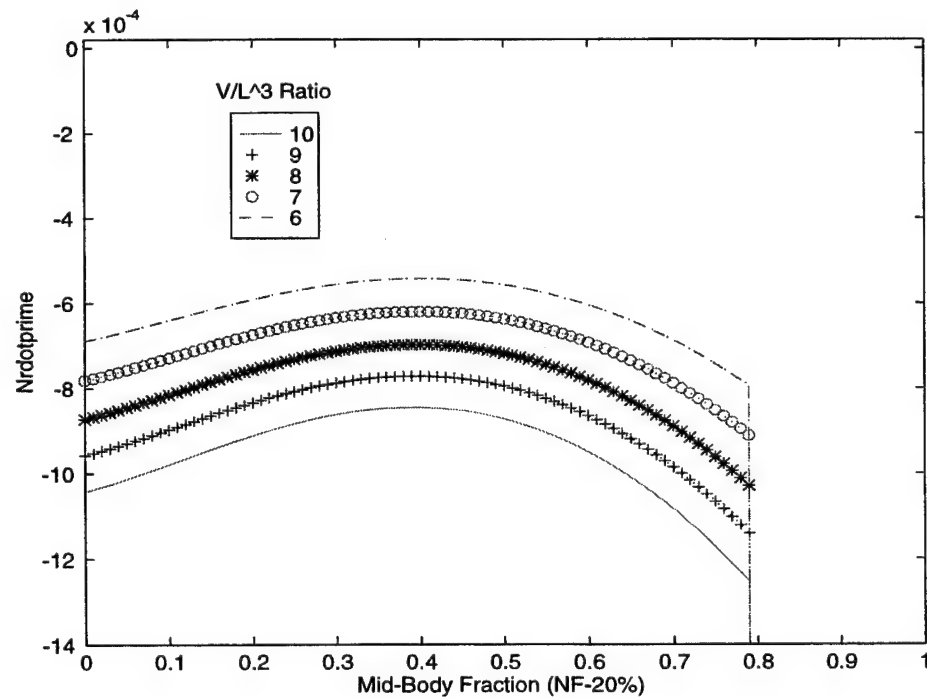


Figure 46. Nrdprime V/L^3 variations at 20% nose fraction.

IV. DETERMINATION OF FUNCTIONAL COEFFICIENTS

A. INTRODUCTION

The hydrodynamic coefficients for various combinations of sectional fractions and volume/length ratios have now been computed and graphed. The surface functions were generated using the semi-empirical methods under the following general formula.

$$HC = F\left(F_n, F_m, \frac{V}{L^3}\right) \quad (25)$$

The goal in predicting the hydrodynamic coefficients would be achieved if we could determine the relationship along the surface function based on the variable parameters.

In order to minimize error and simplify the functional relationships we limited the range of the variable parameters and in each case the range of the parameters covers the majority of the cases of interest. The nose fraction range is 5% to 25%. The mid-body fraction is 40% to 60%. The volume/length³ range is 6 to 10×10^{-3} .

In reviewing Figures 18-31, in our range of interest, the curves appear to correspond to a 2nd degree polynomial. In reviewing Figures 33-46, in our range of interest, the curves have a definite linear relationship. The difficulty would be in determining the surface functional relationship based on two parameters since

currently there is no built-in subroutine in the MATLAB program toolbox in use to solve this problem.

B. PREDICTION EQUATION

Hard copy updates and distribution of improvements in software always involves time delays. In corresponding with the Mathworks company I learned that a collection of m-files existed on the internet. I utilized some of these m-files in the development of my graphs (the legend command is not included on the Macintosh MATLAB professional version). I downloaded a surface equation least squares curve fitting program that I could modify to determine the coefficients of the surface function. I tested the program out using a number of different surface functions and concluded the program accurately predicted the correct polynomial function.

Appendix B includes a sample program.

With the functional coefficients determined the hydrodynamic coefficient prediction equation would be as follows:

$$HC = A_1 F_n^2 + A_2 F_n F_m + A_3 F_m^2 + A_4 F_n + A_5 F_m + A_6 + A_7 \left(\frac{V}{L^3} - C_1 \right) \quad (26)$$

The coefficients for the equations are listed in Table 2 for the nose, mid-body fraction and volume/length³ ratio. The constant C₁ is 8.023x10⁻³ and is the nominal value for volume/length³ ratio.

Figures 47 through 60 compare the theoretical surface functions to the predicted surface functions using the same axial scaling. Figures 60 through 67 are included to demonstrate the percentage error of the prediction equation from the theoretical surface function. In general, the percentage error is small with the exception of the Y_r' percentage error but that is due to the relatively smaller magnitude of the Y_r' hydrodynamic coefficient. The acceleration hydrodynamic prediction equations are very accurate.

HC	A 1	A 2	A 3	A 4	A 5	A 6	A 7
Y_v'	-0.0641	-0.0641	-0.0632	0.0670	0.0732	-0.0263	-0.5769
N_v'	0.0277	0.0499	0.0266	-0.0283	-0.0301	-0.0056	-1.6357
Y_r'	-0.0314	-0.0559	-0.0292	0.0310	0.3160	-0.0091	-0.0880
N_r'	-0.0003	0.0040	0.0027	-0.0012	-0.0045	0.0006	-0.1590
Y_v'	0.0002	0.0007	0.0007	-0.0008	-0.0016	-0.0144	-1.8067
N_v'	-0.0002	-0.0007	-0.0007	0.0008	0.0016	0.0144	1.8067
N_r'	-0.0031	-0.0046	-0.0021	0.0031	0.0024	-0.0013	-0.0808

Table 2. Functional Coefficients for prediction equation.

The coefficients of Table 2 are calculated for the following nominal values: nose fraction 15%, mid-body fraction 50%, and the volume/length³ ratio 8.023×10^{-3} . These parameters represent the mid-range values.

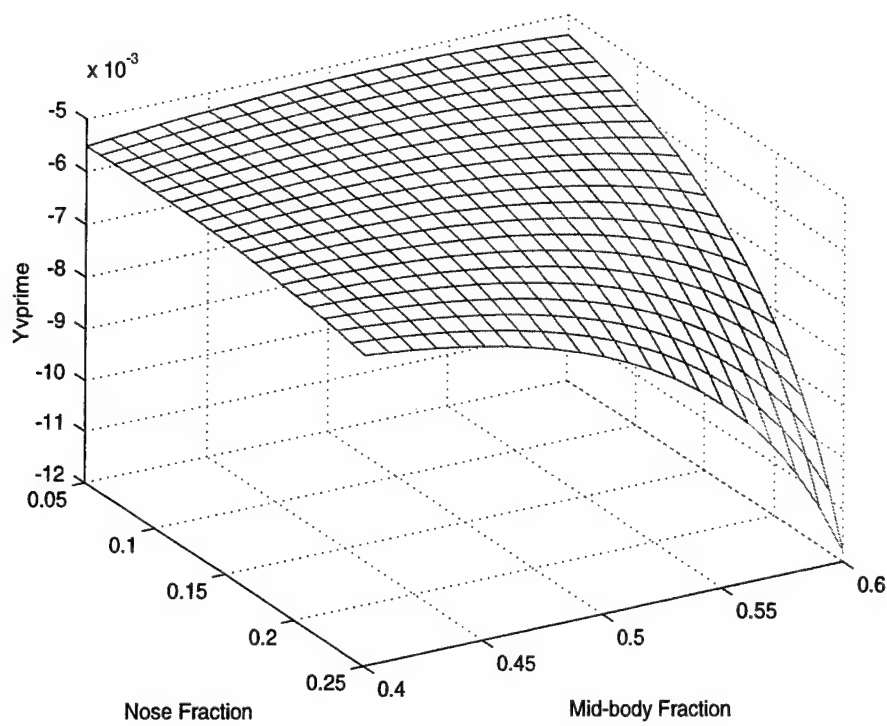


Figure 47. Yvprime theoretical mesh graph.

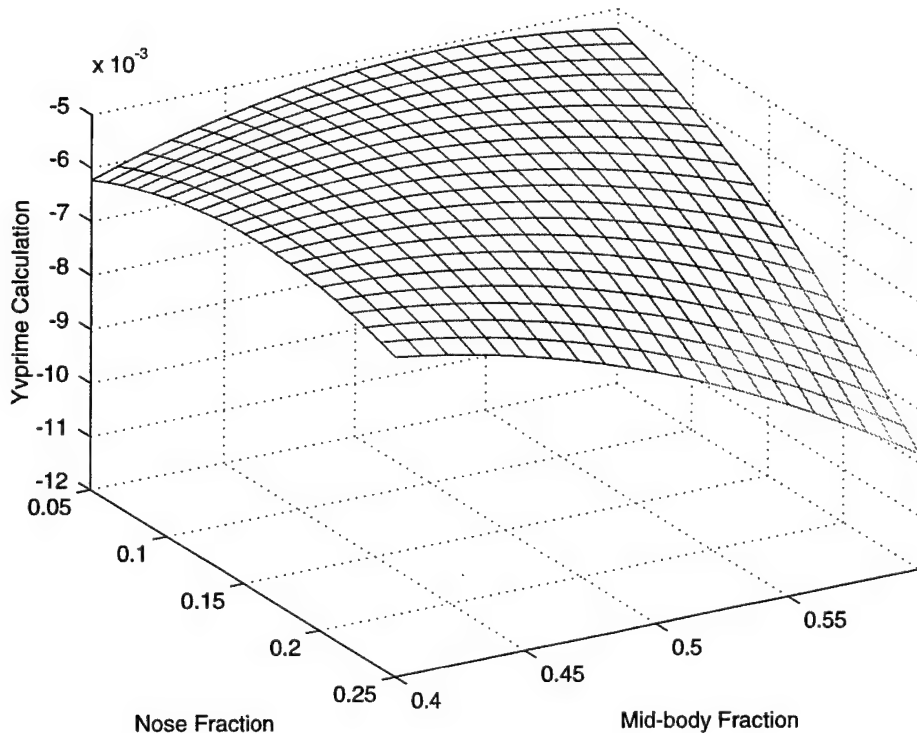


Figure 48. Yvprime predicted mesh graph.

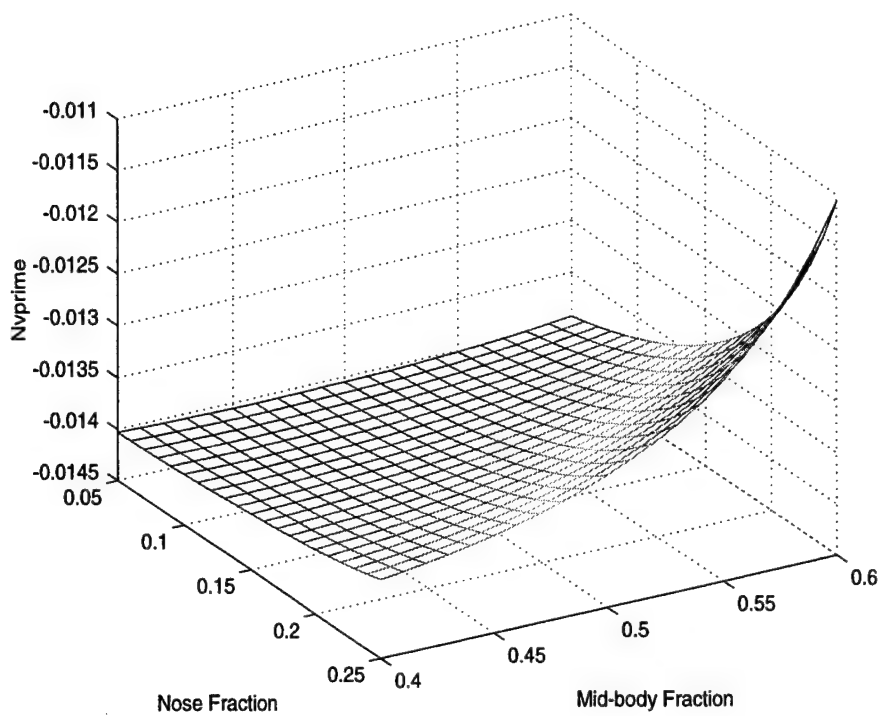


Figure 49. Nvprime theoretical mesh graph.

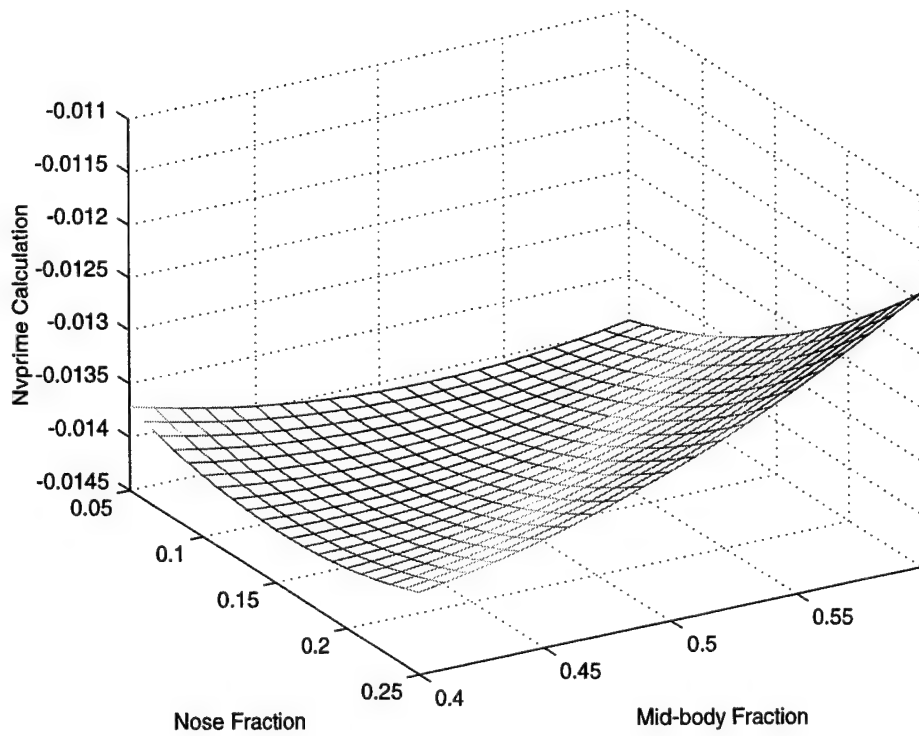


Figure 50. Nvprime predicted mesh graph.

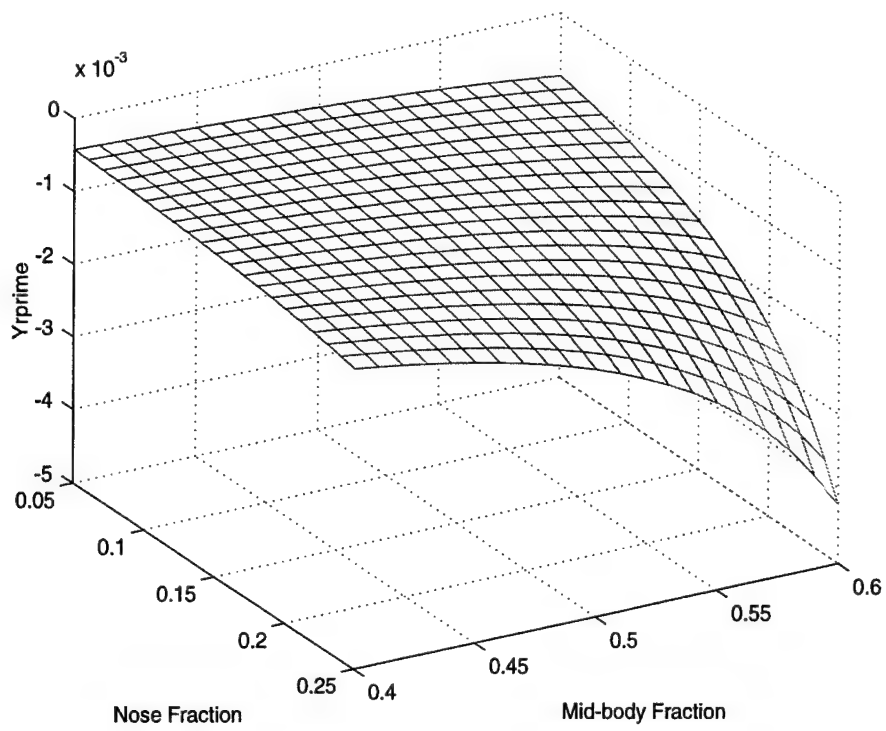


Figure 51. Y_{rprime} theoretical mesh graph.

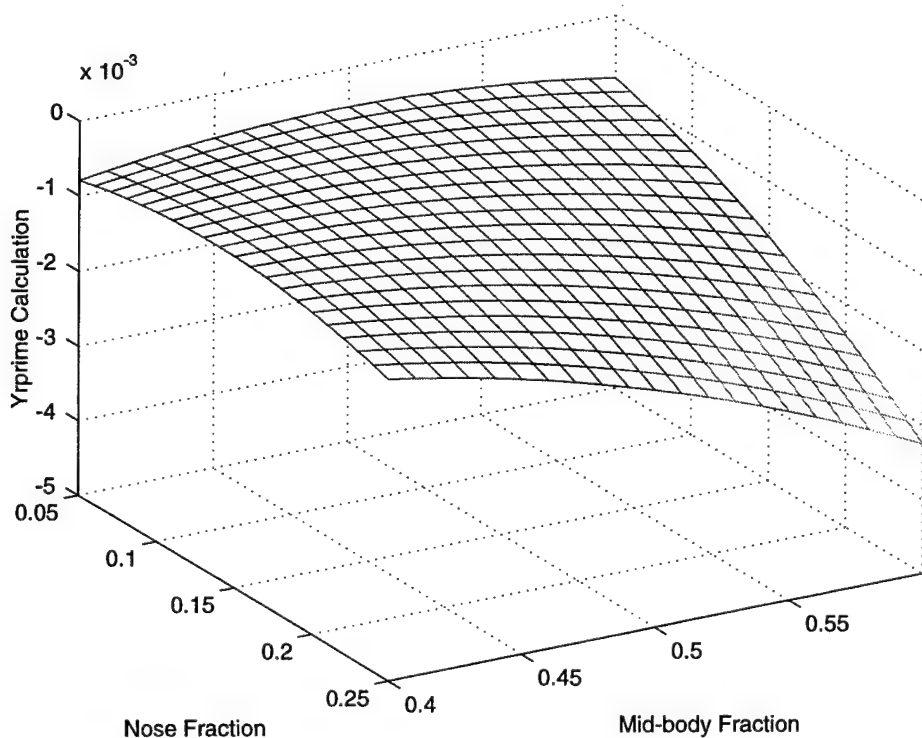


Figure 52. Y_{rprime} predicted mesh graph.

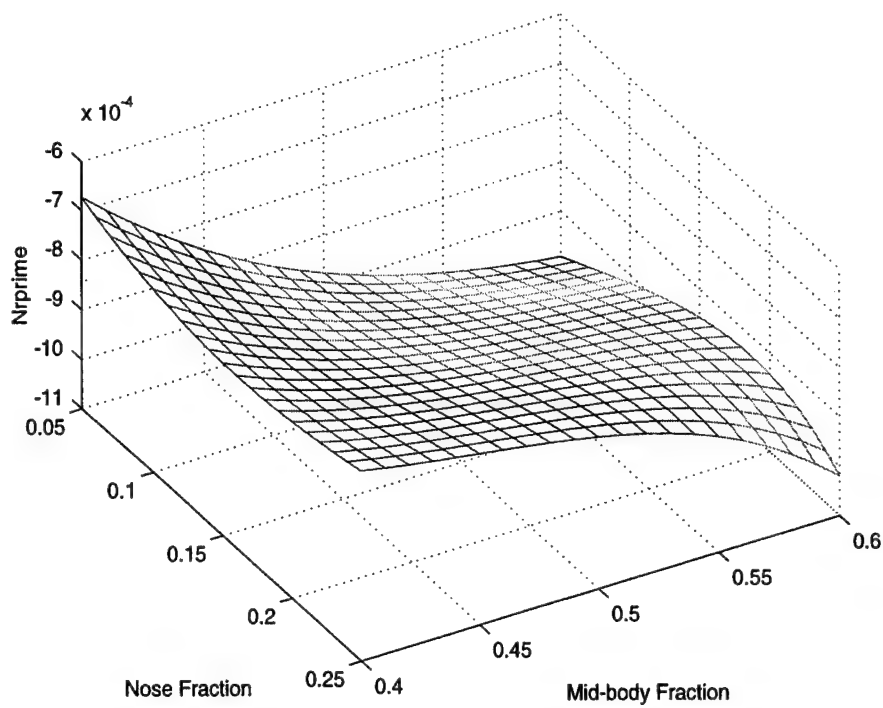


Figure 53. $Nrprime$ theoretical mesh graph.

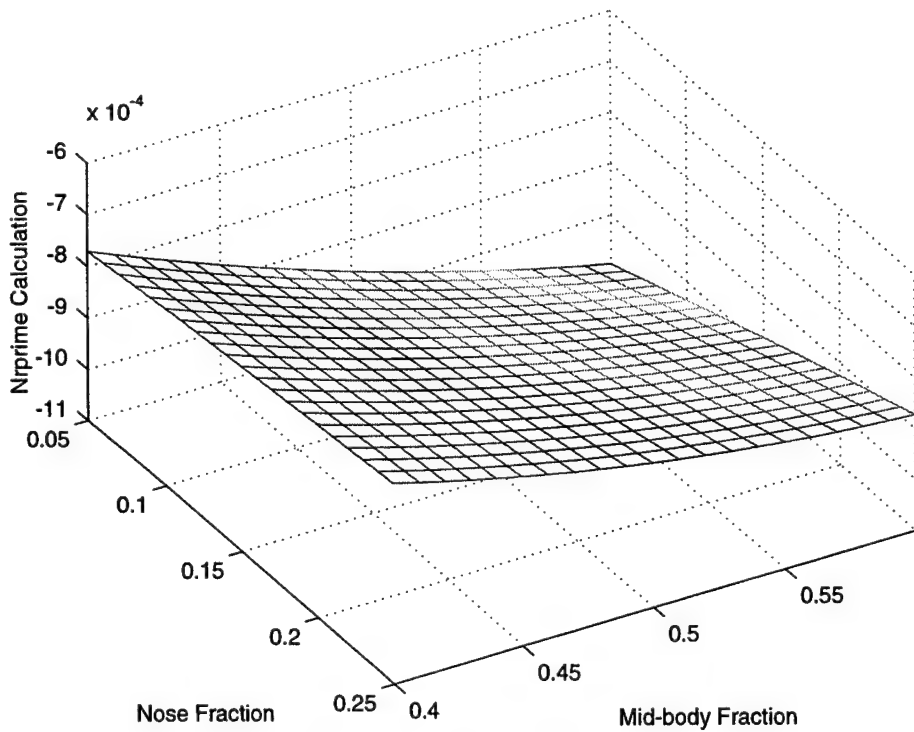


Figure 54. $Nrprime$ predicted mesh graph.

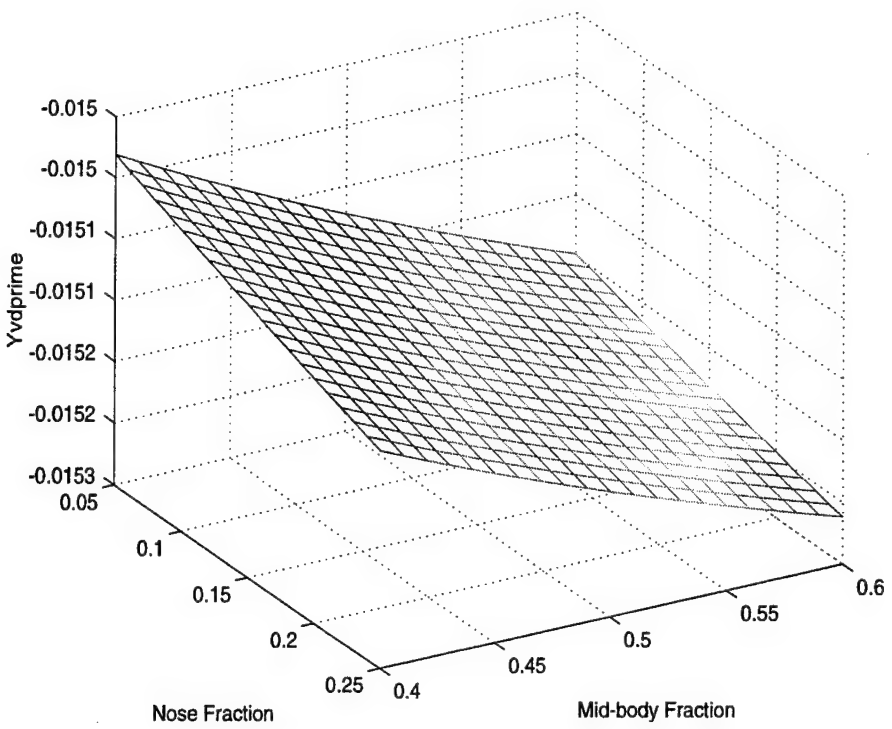


Figure 55. $Y_{vdprime}$ theoretical mesh graph.

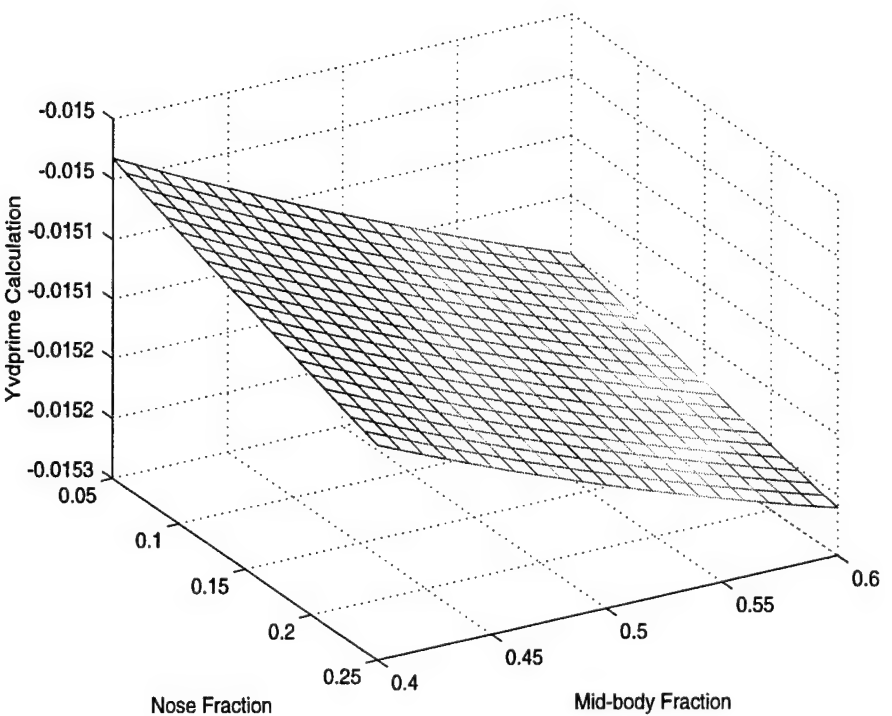


Figure 56. $Y_{vdprime}$ predicted mesh graph.

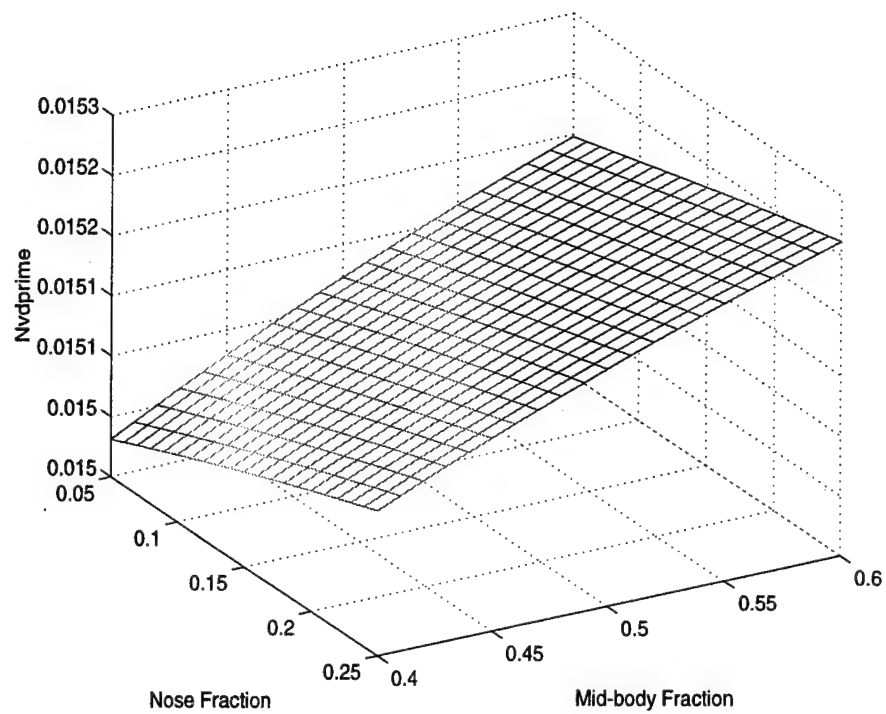


Figure 57. Nvdprime theoretical mesh graph.

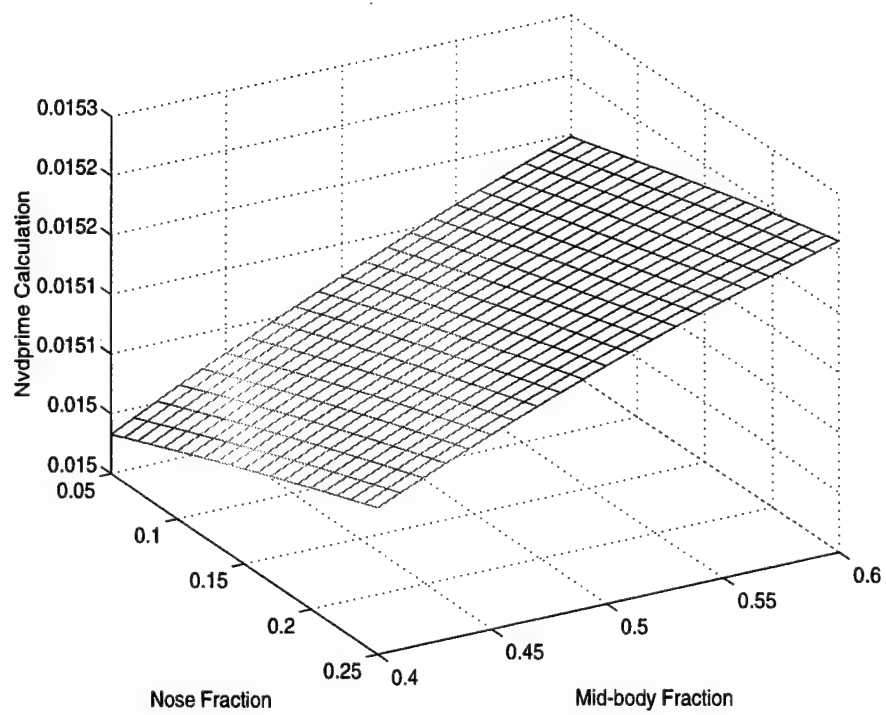


Figure 58. Nvdprime predicted mesh graph.

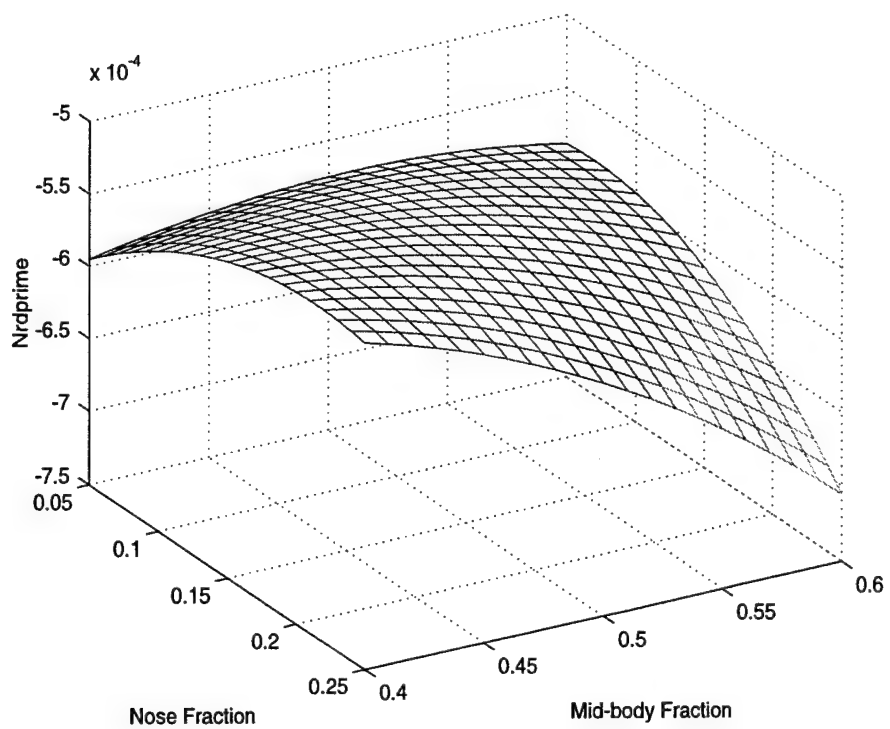


Figure 59. $Nrdprime$ theoretical mesh graph.

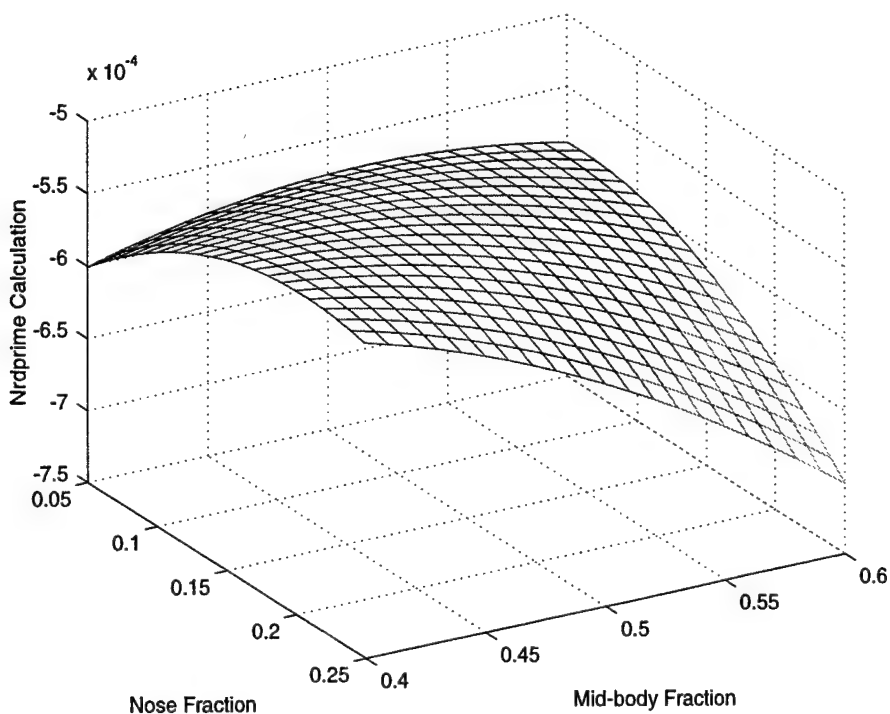


Figure 60. $Nrdprime$ predicted mesh graph.

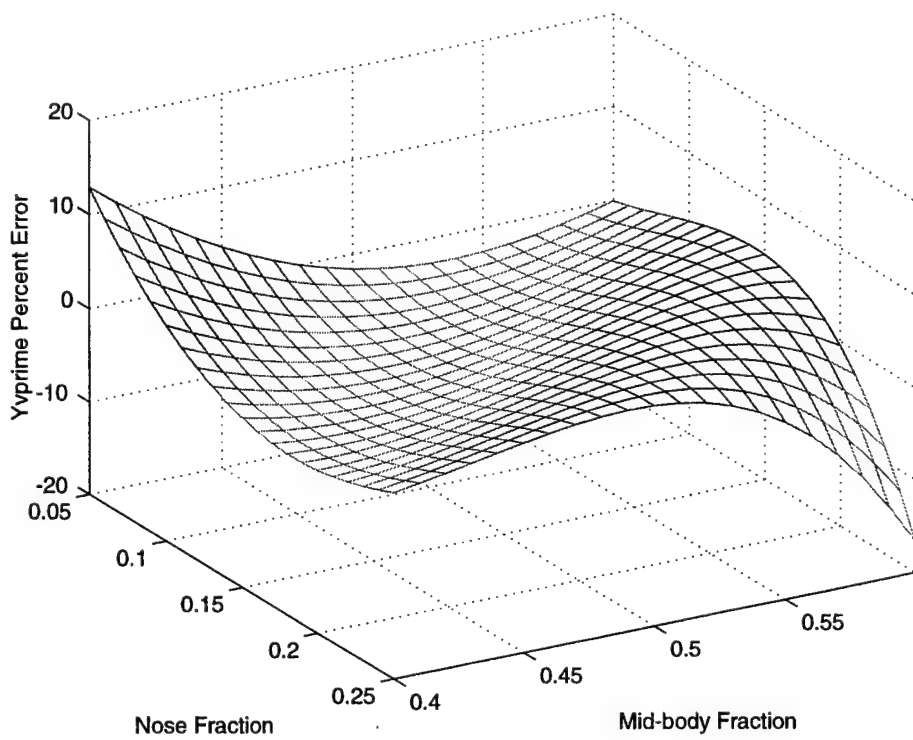


Figure 61. Yprime equation percentage error.

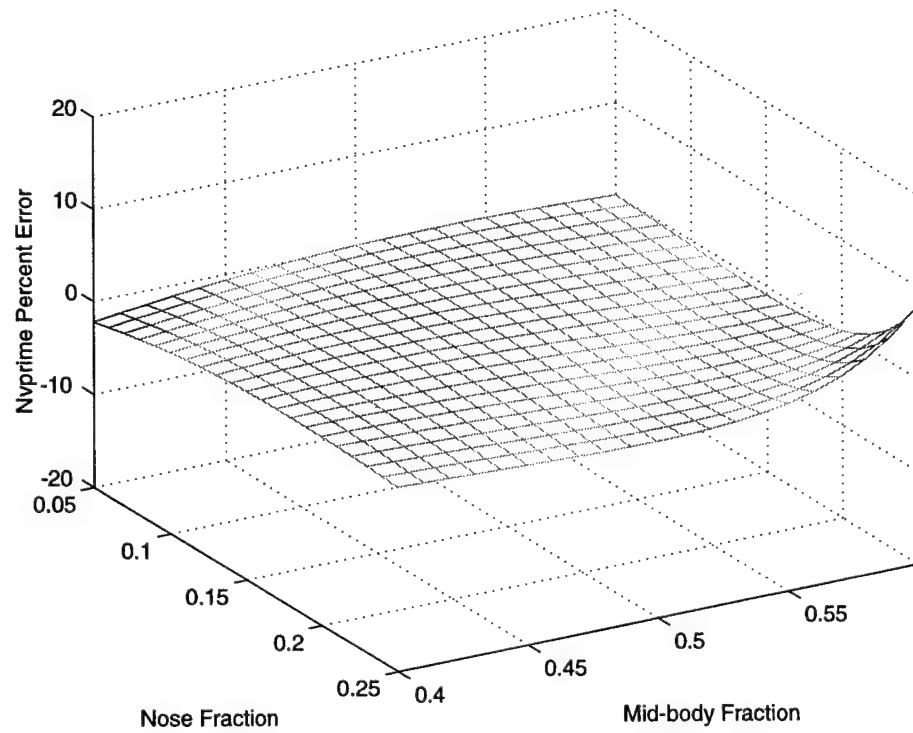


Figure 62. Nvprime equation percentage error.

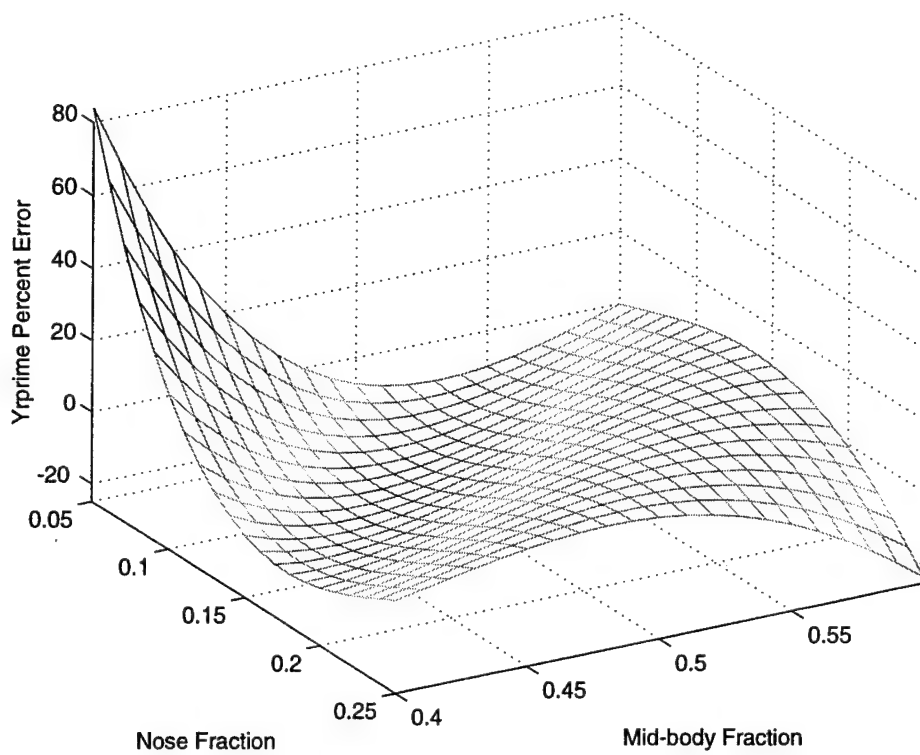


Figure 63. Yrprime equation percentage error.

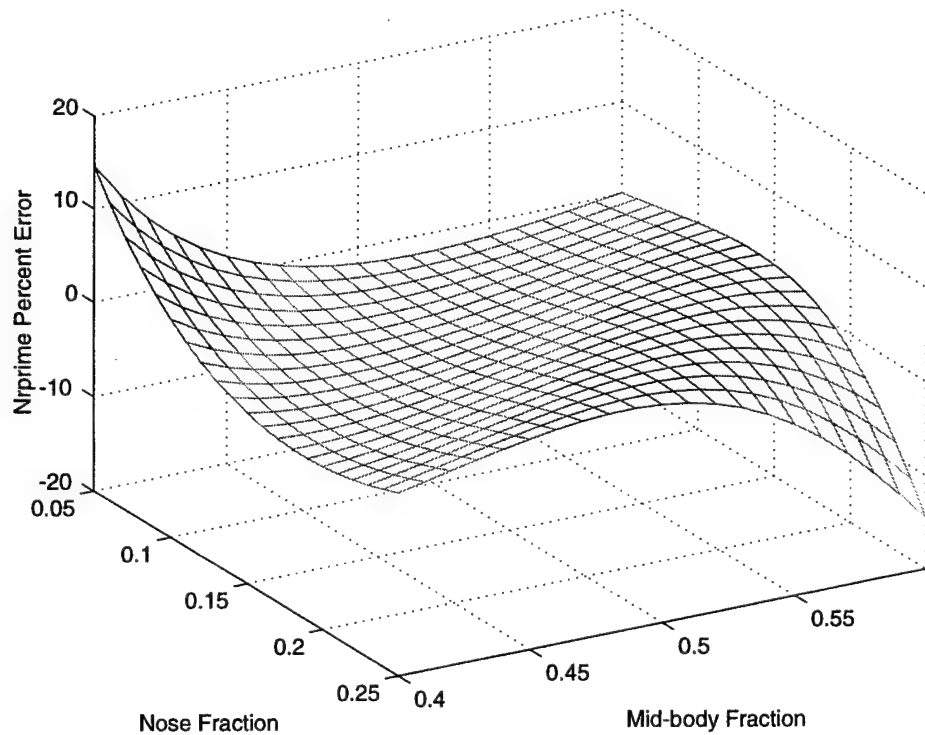


Figure 64. Nrprime equation percentage error.

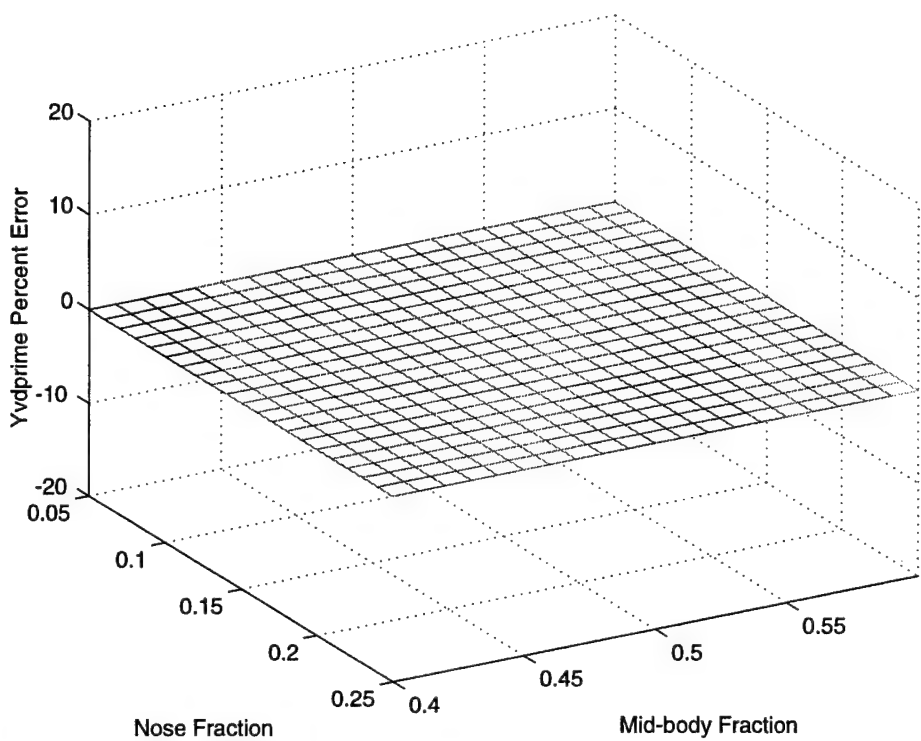


Figure 65. $Y_{vdprime}$ equation percentage error.

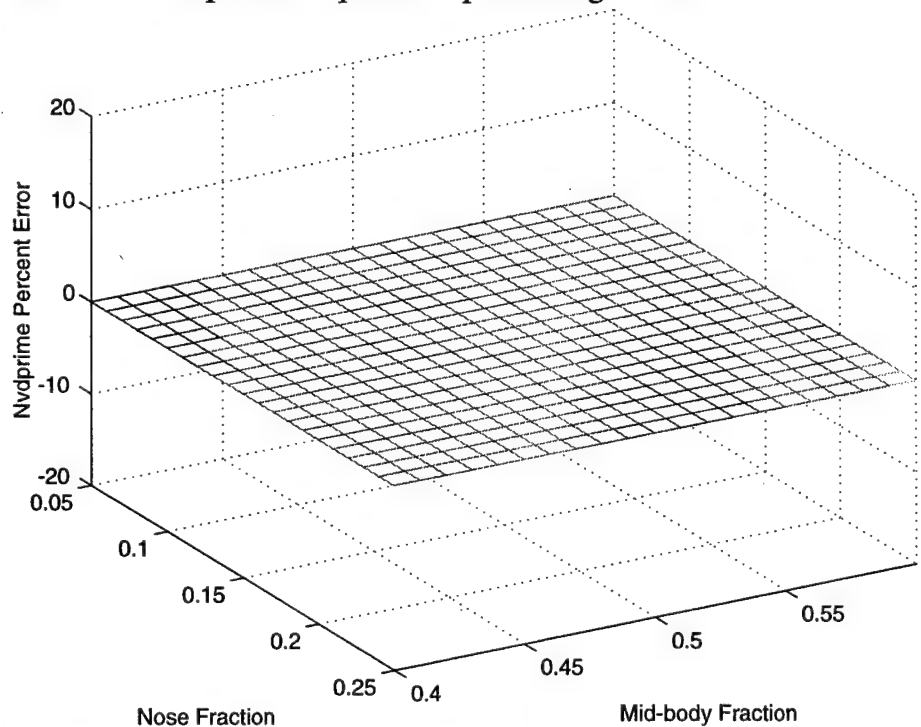


Figure 66. $N_{vdprime}$ equation percentage error.

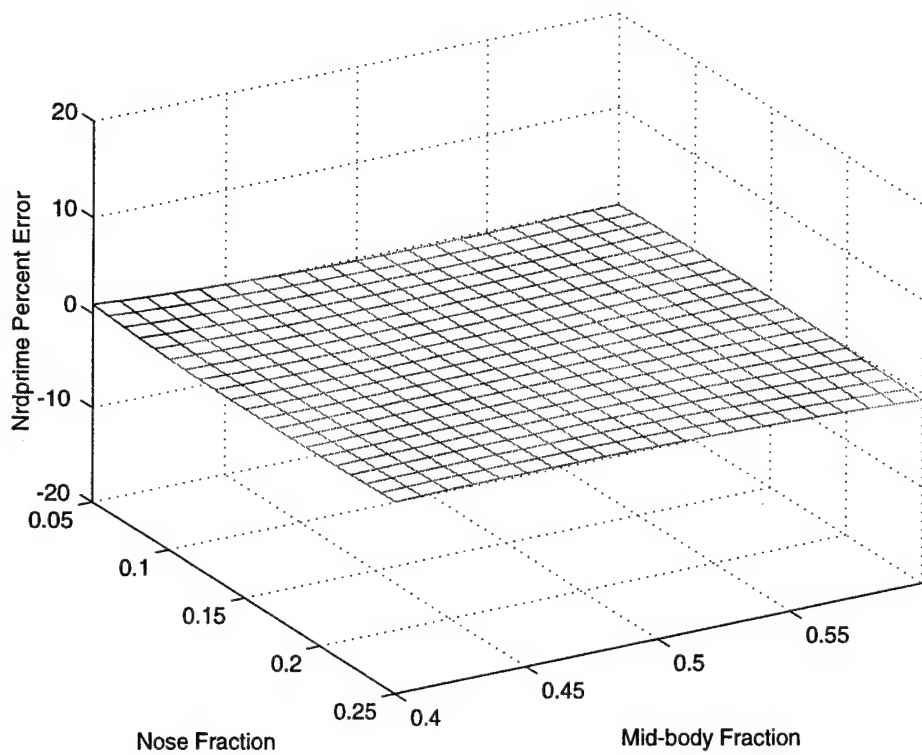


Figure 67. Nrdotprime equation percentage error.

V. CONCLUSIONS AND RECOMMENDATIONS

A. CONCLUSIONS

1. Summary Review of Parameter Variations

The matrix variations of the nose and mid-body fractions resulted in a mixture of surface functions for the hydrodynamic coefficients. There was not an overriding trend that was consistent with all the hydrodynamic coefficients. The trends were all 2nd order polynomials for sectional fractions and linear for volume/length ratio variations. The larger prediction error for the Y_r is due to the relatively smaller magnitude variation in the hydrodynamic coefficient. The acceleration hydrodynamic coefficients were well behaved functions and the prediction equations are highly accurate. The acceleration hydrodynamic coefficients also did not vary greatly in magnitude. Therefore, the designer can alter the sectional fractions without too great a concern for the effects due to acceleration.

A lower volume/length value reduces the magnitude of the hydrodynamic coefficient and this is consistent for all the cases studied. For a constant volume, a lower volume/length implies a longer slimmer body, and a higher slenderness ratio. This would imply the effect of the diameter on the body has a greater impact than the length.

2. Final Comparison

We compared the program results to the expected parameters of the SUBOFF Body and the Slice Pod. The results are listed in Table 3.

HC	SUBOFF Body			Slice Pod		
	Expected	Predicted	% Error	Expected	Predicted	% Error
Y_V'	-0.0058	-0.0054	6.8	-0.0141	-0.0153	7.8
N_V'	-0.0136	-0.0140	2.8	-0.0395	-0.0410	3.6
Y_r'	-0.0014	-0.0008	42.8	-0.0014	-0.0021	30.0
N_r'	-0.0015	-0.0018	18.2	-0.0035	-0.0034	2.9
$Y_{\dot{V}}'$	-0.0152	-0.0151	0.7	-0.0442	-0.0458	3.5
$N_{\dot{V}}'$	0.0152	0.0151	0.7	0.0442	0.0458	3.5
N_r'	-0.0007	0.0006	14.2	-0.0018	-0.0019	5.2

Table 3. Program Comparison.

Overall, the comparison is acceptable with the understanding that the percentage error with N_r' is due to its relatively small value. The Y_r' percentage error is within the tolerance of the program.

B. RECOMMENDATIONS

The parametric study of the body of revolution while singular in scope presents the ability to pursue variations in the design of components and their effect on the hydrodynamic coefficients.

Recommendations for further research in this area are as follows:

- Modify the program to evaluate different shapes.
- Evaluate motion in the vertical plane.
- Calculate stability criteria and general maneuvering performance for the surface mesh functions.

APPENDIX A. MATLAB ROUTINE FOR DETERMINING HYDRODYNAMIC COEFFICIENTS WITH VARYING NOSE AND MID-BODY FRACTIONS

A. VDCURVES.M PROGRAM

```
% LCDR Eric Holmes
% Constant: Volume/Length^3 ratio
% Thesis

clear
clear global

% Basic Parameters

% lB = Total body length
% ln = Nose length
% lm = Middle body length
% lb = Base body length
% d = diameter
% lf = forebody length (lb + lm)
% Fn = Nose fractional length of total body length
% Fm = Mid-body fractional length of total body length
% r_Fm = maximum fraction of mid-body
% Fb = Base fractional length of total body length
% N,I,k,t = index counters
% Sb = maximum cross sectional area of body (assuming diameter
%       d and length lB)
% V = Volume of the body
% xm = Geometric middle of body
% xcb = Geometric offset from the center of the middle body
%       for gravity
% lcb = Geometric center of gravity
% rho = density of water
% e = Munk coefficient
% Bo = Munk coefficient
% Ao = Munk coefficient
% k1 = Lamb's inertial coefficient
% k2 = Lamb's inertial coefficient
% kb = Lamb's inertial coefficient
% Cdo = Drag coefficient at zero angle of attack
```

```

% lv = length where viscous flow dominates
% r = radius at length lv
% R = range for graphs
% S = Slenderness ratio matrix
% Sratio = slenderness ratio
% Sv = cross sectional area at length lv
% Stb = platform sectional area at length lv
% Cla = Lift/Angle of attack curve slope
% Cma = Pitching moment/Angle of attack curve slope
% Cmq = Pitching moment/pitch rate curve slope
% Clq = Lift/Pitch rate curve slope
% Iydf = mass moment of inertia of displaced fluid mass
% Iydf_In = nose body component of Iydf
% Iydf_lm = middle body component of Iydf
% Iydf_lb = base body component of Iydf

% Hydrodynamic coefficients
% Yvprime = normal force coefficient
% Nvprime = pitching moment coefficient
% Yrprime = normal force/pitch rate coefficient
% Nrprime = pitching moment/pitch rate coefficient
% Zwdotprime = acceleration coefficient (axisymmetric to Yvdotprime)
% Yvdotprime = acceleration coefficient along y axis
% Nvdotprime = acceleration coefficient causing yawing moments
% Nrdotprime = acceleration coefficient in addition to Iz

% Yvp,Nvp,Yrp,Nrp,Yvdp,Nvdp,Nrdp are hydrodynamic
% coefficient matrices each combining the values of their respective
% coefficient: Yvpprime => Yvp
% Yvp_d,Nvp_d,Yrp_d,Nrp_d,Yvdp_dNvp_d,Nrp_d are hydrodynamic
% coefficient matrices maintained as raw data.
% (The matrix filler is -1.0)
% Yvp_s,Nvp_s,Yrp_s,Nrp_s,Yvdp_s,Nvp_s,Nrp_s are hydrodynamic
% coefficient matrices that have been clipped for graphical
% presentation

% Initializing data and empty matrices

```

S = []; Yvp = []; Nvp = []; Yrp = []; Nrp = []; Yvdp =[]; Nvdp = []; Nrdp = [];

R = (0:0.01:1);

```
V = 1;  
lB = 4.9941;  
rho = 62.4/32.174;
```

% Drag Function Development

```
ln_d = [0 .5 1 1.5 2 2.5 3];  
cd_lnd = [0.82 .45 .29 .29 .29 .29];  
cln = polyfit(ln_d,cd_lnd,4);
```

```
lb_d = [0 .5 1 1.5 2 2.5 3];  
cd_lbd = [0.64 .38 .29 .29 .29 .29];  
clb = polyfit(lb_d,cd_lbd,4);
```

% Establishing fractional values for the body

```
Fn = (0:0.01:1);  
for k = 1:101;  
r_Fm = 1 - Fn(k);  
  
Fm = (0:0.01:r_Fm);  
Fb = 1 - Fn(k) - Fm;
```

% Diameter calculation

```
d = ((12*V)./((pi*lB).*(2*Fn(k) + 3*Fm + Fb))).^0.5;
```

% Length calculation

```
ln = Fn(k).*lB;  
lm = Fm.*lB;  
lb = Fb.*lB;  
lf = ln + lm;
```

% Slenderness ratio calculation

```
Sratio = lB./d;  
S = [S zeros(1,k-1)];
```

% Body calculation

```

Sb = (pi.*d.^2)/4;
xm = lB/2;

global d lB lf ln lm lb xm rho I

% Center of gravity and bouyancy

xcb = (pi*d.^2./12).*((2.*ln.*((lm/2 + 3*ln/8) - lb.*((lm/2 + 3*lb/4)))/V;

lcb = ln + lm/2 - xcb;

% Munk coefficients

e = (2./lB).*(((lB.^2)/4 - Sb/pi)).^0.5;
Bo = (1./e.^2) - ((1 - e.^2)./(2*e.^3)).*log((1+e)./(1-e));
Ao = ((1-(e.^2))./(e.^3)).*(log((1+e)./(1-e)) - 2*e);
k1 = Ao./(2 - Ao);
k2 = Bo./(2 - Bo);
kb = ((e.^4).*(Bo - Ao))./((2 - e.^2).*(2*e.^2 - (2 - e.^2).*(Bo - Ao)));

% Normal force coefficients

% Drag coefficient determination

for i = 1:102 - k
if ln/d(i) < 1
    Cdo(i) = cln(1)*(ln/d(i))^4 + cln(2)*(ln/d(i))^3 + cln(3)*(ln/d(i))^2 + ...
               cln(4)*(ln/d(i)) + cln(5);
else
    Cdo(i) = 0.29;
end
if lb(i)/d(i) < 1
    Cdo(i) = clb(1)*(lb(i)/d(i))^4 + clb(2)*(lb(i)/d(i))^3 + ...
               clb(3)*(lb(i)/d(i))^2 + clb(4)*(lb(i)/d(i)) + clb(5);
else
    Cdo(i) = 0.29;
end
end

lv = 0.905*lB;

r = (d./2).*(1 - (lv - lf)./lb);

```

```

Sv = pi.*r.^2;
Cla = (2*(k2 - k1).*Sv)./Sb;
Yvprime = (-Sb./lB.^2).*(Cla + Cdo);

Yvp = [Yvp Yvprime -(ones(1,k-1))];

Cma = (2*(k2-k1)./(Sb*lB)).*((-pi.*d.^2./12).* (3*xm - ln) + ...
((pi.*d.^2)./(12*lB.^2)).* ...
(-3*xm.*lv.^2 + 6*lv.*xm.*lb + 2*lv.^3 - 3*lf.*lv.^2 - 3*lb.*lv.^2 + ...
6*lv.*xm.*lf - 6*lf.*xm.*lb + 3*lb.*lf.^2 - 3*xm.*lf.^2 + lf.^3));

Nvprime = (Sb.*Cma)./lB.^2;

Nvp = [Nvp Nvprime -(ones(1,(k-1))];

% Rotary force coefficients

Stb = r.* (lB - lv);

Cmq = Cma.*((1 - xm./lB).^2 - V*(lcb - xm)./(Stb.*lB.^2))./...
((1 - xm./lB) - (V./(Stb.*lB)));

Nrprime = -(Sb.*Cmq)./lB.^2;

Nrp = [Nrp Nrprime -(ones(1,(k-1))];
clear Nrprime

Clq = Cla.* (1 - xm./lB);

Yrprime = (-Sb.*Clq)./lB.^2;

Yrp = [Yrp Yrprime -(ones(1,(k-1))];

% Acceleration coefficients

Zwdotprime = (2*k2*V)./(lB.^3);

Yvdotprime = -Zwdotprime;

Yvdp = [Yvdp Yvdotprime -(ones(1,(k-1))];

```

```

for I = 1:102-k;

Iydf_ln(I) = quad8('vdn',0,ln);
Iydf_lm(I)= quad8('vdm',ln,lf(I));
Iydf_lb(I) = quad8('vdb',lf(I),lB);

end

Iydf = Iydf_ln + Iydf_lm + Iydf_lb;

Nrdotprime = (-2.*kb.*Iydf)./(rho.*lB.^5);

Nrdp = [Nrdp Nrdotprime -(ones(1,(k-1)))] ;

N = isnan(Nrdp);
I = find(N > 0);
for t = 1:length(I)
    Nrdp(I(t)) = -1.0;
end

clear d lf ln lm lb xm I
clear Iydf_ln Iydf_lm Iydf_lb Iydf
clear global
lB = 4.9941;
rho = 62.4/32.174;

end

Nvdp = -Yvdp;
Nvdp = reshape(Nvdp,101,101);

Yvp_d = reshape(Yvp,101,101);
Nvp_d = reshape(Nvp,101,101);
Yrp_d = reshape(Yrp,101,101);
Nrp_d = reshape(Nrp,101,101);
Yvdp_d = reshape(Yvdp,101,101);
Nvdp_d = reshape(Nvdp,101,101);
Nrdp_d = reshape(Nrdp,101,101);

save Yvp_d Nvp_d Yrp_d Nrp_d Yvdp_d Nvdp_d Nrdp_d

```

```

% Format for presentation (all analysis complete)

Nvp = reshape(Nvp,101,101);

figure(1)
plot(R,Nvp(1:101,6),'c', R,Nvp(1:101,11),'r+', R,Nvp(1:101,16),'b*', ...
    R,Nvp(1:101,21),'go')
xlabel('Mid-body Fraction')
ylabel('Nvprime')
text(0.1,-0.0132,'Nose Fraction (%)')
legend(' 5','10','15','20')
axis([0 1 -0.0145 -0.013])
hold on
plot(R,Nvp(1:101,11),'r', R,Nvp(1:101,16),'b', R,Nvp(1:101,21),'g')
hold off
pause
print -depsc2 nvp

Nvp = reshape(Nvp,1,10201);
k = find(Nvp > -0.01);
Nvp(k) = -0.02*(ones(length(k),1));
Nvp = reshape(Nvp,101,101);

k = find(Nrp < -0.01);
Nrp(k) = ones(length(k),1);
Nrp = reshape(Nrp,101,101);

figure(2)
plot(R,Nrp(1:101,6),'c', R,Nrp(1:101,11),'r+', R,Nrp(1:101,16),'b*', ...
    R,Nrp(1:101,21),'go')
xlabel('Mid-body Fraction')
ylabel('Nrprime')
text(0.2,0.0025,'Nose Fraction (%)')
legend(' 5','10','15','20')
axis([0 1 -0.0025 0.003])
hold on
plot(R,Nrp(1:101,11),'r', R,Nrp(1:101,16),'b', R,Nrp(1:101,21),'g')
hold off
pause
print -depsc2 nrp

```

```

Nrp = reshape(Nrp,1,10201);
k = find(Nrp > 0.05);
Nrp(k) = -0.02*(ones(length(k),1));
Nrp = reshape(Nrp,101,101);

figure(3)
plot(R,Nrdp(1:101,6),'c', R,Nrdp(1:101,11),'r+', R,Nrdp(1:101,16),'b*', ...
      R,Nrdp(1:101,21),'go')
xlabel('Mid-body Fraction')
ylabel('Nrdotprime')
text(0.6,-0.00015,'Nose Fraction (%)')
legend(' 5','10','15','20')
axis([0 1 -0.0012 0])
hold on
plot(R,Nrdp(1:101,11),'r+', R,Nrdp(1:101,16),'b:', R,Nrdp(1:101,21),'g:')
hold off
pause
print -depsc2 nrdf

k = find(Nrdp < -0.02);
Nrdp(k) = -0.02*(ones(length(k),1));
Nrdp = reshape(Nrdp,101,101);

k = find(Yvp<-0.02);
Yvp(k) = -0.02*(ones(length(k),1));
Yvp = reshape(Yvp,101,101);

k = find(Yrp < -0.02);
Yrp(k) = -0.02*(ones(length(k),1));
Yrp = reshape(Yrp,101,101);

k = find(Yvdp < -0.02);
Yvdp(k) = -0.02*(ones(length(k),1));
Yvdp = reshape(Yvdp,101,101);

figure(4)
plot(R,Yvp(1:101,6),'c', R,Yvp(1:101,11),'r+', R,Yvp(1:101,16),'b*', ...
      R,Yvp(1:101,21),'go')
xlabel('Mid-body Fraction')
ylabel('Yvprime')
text(0.15,-0.0075,'Nose Fraction (%)')
legend(' 5','10','15','20')

```

```

axis([0 1 -0.01 -0.004])
hold on
plot(R,Yvp(1:101,11),'r:', R,Yvp(1:101,16),'b:', R,Yvp(1:101,21),'g:')
hold off
pause
print -depsc2 yvp

figure(5)
plot(R,Yrp(1:101,6),'c', R,Yrp(1:101,11),'r+', R,Yrp(1:101,16),'b*', ...
      R,Yrp(1:101,21),'go')
xlabel('Mid-body Fraction')
ylabel('Yrprime')
text(0.15,-0.0025,'Nose Fraction (%)')
legend(' 5','10','15','20')
axis([0 1 -0.005 0])
hold on
plot(R,Yrp(1:101,11),'r:', R,Yrp(1:101,16),'b:', R,Yrp(1:101,21),'g:')
hold off
pause
print -depsc2 yrp

figure(6)
plot(R,Yvdp(1:101,6),'c', R,Yvdp(1:101,11),'r+', R,Yvdp(1:101,16),'b*', ...
      R,Yvdp(1:101,21),'go')
xlabel('Mid-body Fraction')
ylabel('Yvdotprime')
text(0.5,-0.0146,'Nose Fraction (%)')
legend(' 5','10','15','20')
axis([0 1 -0.0154 -0.0145])
hold on
plot(R,Yvdp(1:101,11),'r:', R,Yvdp(1:101,16),'b:', R,Yvdp(1:101,21),'g:')
hold off
pause
print -depsc2 yvdp

figure(7)
plot(R,Nvdp(1:101,6),'c', R,Nvdp(1:101,11),'r+', R,Nvdp(1:101,16),...
      'b*', R,Nvdp(1:101,21),'go')
xlabel('Mid-body Fraction')
ylabel('Nvdotprime')
text(0.4,0.015,'Nose Fraction (%)')
legend(' 5','10','15','20')

```

```

axis([0 1 0.0145 0.0154])
hold on
plot(R,Nvdp(1:101,11),'r:', R,Nvdp(1:101,16),'b:', R,Nvdp(1:101,21),'g:')
hold off
pause
print -depsc2 nvdp

% Range change for mesh graphics

R = (0:0.02:1);

figure(8)
S = reshape(S,101,101);
mesh(R,R,S(1:2:101,1:2:101)),grid
xlabel('Nose Fraction')
ylabel('Mid-body Fraction')
zlabel('Slenderness Ratio')
view(60,30)
print -depsc2 slender

figure(9)
mesh(R,R,Yvp(1:2:101,1:2:101)), grid
xlabel('Nose Fraction')
ylabel('Mid-body Fraction')
zlabel('Yvprime')
view(60,30)
print -depsc2 yvpm

figure(10)
mesh(R,R,Nvp(1:2:101,1:2:101)), grid
xlabel('Nose Fraction')
ylabel('Mid-body Fraction')
zlabel('Nvprime')
view(40,40)
print -depsc2 nvp

figure(11)
mesh(R,R,Yrp(1:2:101,1:2:101)), grid
xlabel('Nose Fraction')
ylabel('Mid-body Fraction')
zlabel('Yrprime')
view(60,30)

```

```

print -depsc2 yrpm

figure(12)
mesh(R,R,Nrp(1:2:101,1:2:101)), grid
xlabel('Nose Fraction')
ylabel('Mid-body Fraction')
zlabel('Nrprime')
view(40,30)
print -depsc2 nrpm

figure(13)
mesh(R,R,Yvdp(1:2:101,1:2:101)), grid
xlabel('Nose Fraction')
ylabel('Mid-body Fraction')
zlabel('Yvdotprime')
view(60,30)
print -depsc2 yvdpm

figure(14)
mesh(R,R,Nvdp(1:2:101,1:2:101)), grid
xlabel('Nose Fraction')
ylabel('Mid-body Fraction')
zlabel('Nvdotprime')
view(20,20)
print -depsc2 nvdpm

figure(15)
mesh(R,R,Nrdp(1:2:101,1:2:101)), grid
xlabel('Nose Fraction')
ylabel('Mid-body Fraction')
zlabel('Nrdotprime')
view(60,50)
print -depsc2 nrdpm

% Clipping of data for graphical presentation

Yvp_s = reshape(Yvp,1,10201);
k = find(Yvp_s<-0.01);
Yvp_s(k) = -0.01*(ones(length(k),1));
Yvp_s = reshape(Yvp_s,101,101);

Nvp_s = reshape(Nvp,1,10201);

```

```

k = find(Nvp_s > -0.013);
Nvp_s(k) = -0.0145*(ones(length(k),1));
k = find(Nvp_s < -0.0145);
Nvp_s(k) = -0.0145*(ones(length(k),1));
Nvp_s = reshape(Nvp_s,101,101);

Yrp_s = reshape(Yrp,1,10201);
k = find(Yrp_s < -0.005);
Yrp_s(k) = -0.005*(ones(length(k),1));
Yrp_s = reshape(Yrp_s,101,101);

Nrp_s = reshape(Nrp,1,10201);
k = find(Nrp_s < -0.005);
Nrp_s(k) = -0.005*(ones(length(k),1));
Nrp_s = reshape(Nrp_s,101,101);

Yvdp_s = reshape(Yvdp,1,10201);
k = find(Yvdp_s < -0.0154);
Yvdp_s(k) = -0.0154*(ones(length(k),1));
Yvdp_s = reshape(Yvdp_s,101,101);

Nvdp_s = -Yvdp_s;

Nrdp_s = reshape(Nrdp,1,10201);
k = find(Nrdp_s < -0.00125);
Nrdp_s(k) = -0.00125*(ones(length(k),1));
Nrdp_s = reshape(Nrdp_s,101,101);

figure(16)
mesh(R,R,Yvp_s(1:2:101,1:2:101)), grid
xlabel('Nose Fraction')
ylabel('Mid-body Fraction')
zlabel('Yvprime')
view(60,30)
print -depsc2 yvps

figure(17)
mesh(R,R,Nvp_s(1:2:101,1:2:101)), grid
xlabel('Nose Fraction')
ylabel('Mid-body Fraction')
zlabel('Nvprime')
view(40,40)

```

```

print -depsc2 nvpss

figure(18)
mesh(R,R,Yrp_s(1:2:101,1:2:101)), grid
xlabel('Nose Fraction')
ylabel('Mid-body Fraction')
zlabel('Yrprime')
view(60,30)
print -depsc2 yrps

figure(19)
mesh(R,R,Nrp_s(1:2:101,1:2:101)), grid
xlabel('Nose Fraction')
ylabel('Mid-body Fraction')
zlabel('Nrprime')
view(40,40)
print -depsc2 nrps

figure(20)
mesh(R,R,Yvdp_s(1:2:101,1:2:101)), grid
xlabel('Nose Fraction')
ylabel('Mid-body Fraction')
zlabel('Yvdotprime')
view(60,30)
print -depsc2 yvdps

figure(21)
mesh(R,R,Nvdp_s(1:2:101,1:2:101)), grid
xlabel('Nose Fraction')
ylabel('Mid-body Fraction')
zlabel('Nvdotprime')
view(40,30)
print -depsc2 nvdpss

figure(22)
mesh(R,R,Nrdp_s(1:2:101,1:2:101)), grid
xlabel('Nose Fraction')
ylabel('Mid-body Fraction')
zlabel('Nrdotprime')
axis([0 1 0 1 -0.00125 -0.0005])
view(60,50)
print -depsc2 nrdps

```

B. VDN.M PROGRAM

```
%LCDR Eric Holmes
%Thesis
%Iydf_ln Functional Integration

% d = diameter
% lB = total body length
% ln = nose length
% lm = middle length
% lb = base length
% xm = geometric middle of the body
% rho = density of water

function I1 = vdn(x)

global d lB lf ln lm lb xm rho I

I1 = ((-rho*pi.*d(I).^2.*x.*((xm - x).^2./(4.*ln.^2)).*(x - 2.*ln));
```

C. VDM.M PROGRAM

```
%LCDR Eric Holmes
%Thesis
%Iydf_lm Functional Integration

% d = diameter
% lB = total body length
% ln = nose length
% lm = middle length
% lb = base length
% xm = geometric middle of the body
% rho = density of water

function I2 = vdm(x)

global d lB lf ln lm lb xm rho I

I2 = (rho*pi.*d(I).^2/4).*((xm - x).^2;
```

D. VDB.M PROGRAM

```
%LCDR Eric Holmes
%Thesis
%Iydf_lb Functional Integration

% d = diameter
% lB = total body length
% ln = nose length
% lm = middle length
% lb = base length
% xm = geometric middle of the body
% rho = density of water
% lf = fore body (lb + lm)

function I3 = vdb(x)

global d lB lf ln lm lb xm rho I

I3 = (pi*rho.*d(I).^2.* (xm - x).^2).* (lb(I) - x + lf(I)).^2./(4*lb(I).^2);
```


APPENDIX B. SAMPLE MATLAB ROUTINE FOR DETERMINING FUNCTIONAL COEFFICIENTS FROM A SURFACE PROFILE

A. SURF.M PROGRAM

```
% LCDR Eric P. Holmes  
% Surface Equation Solver
```

```
n = 2;  
x = []; y = [];  
load hcdta  
Yvp = Yvp_d(6:26,41:61);  
Yvp = Yvp(:);
```

```
% Range
```

```
xr = (5:25);  
for i = 1:21  
    x = [x;xr];  
end  
x = 0.01*x;  
x = x(:);
```

```
yr = (40:60);  
for i = 1:21  
    y = [y yr];  
end  
y = 0.01*y;  
y = y(:);
```

```
% Program operation
```

```
n = n+1;  
k = 1;  
A = zeros(size(x));  
for i = n:-1:1,  
    for j = 1:i  
        A(:,k) = ((x.^ (i-j)).*(y.^ (j-1)));  
        k = k+1;  
    end  
end
```

```

p = (A\Yvp).'

% Error calculation

x = reshape(x,21,21);
y = reshape(y,21,21);
Yvp = reshape(Yvp,21,21);

for i = 1:21
    for j = 1:21
        Yvpcal(i,j) = p(1)*x(i,j)^2 + p(2)*x(i,j)*y(i,j) + p(3)*y(i,j)^2 + ...
        p(4)*x(i,j) + p(5)*y(i,j) + p(6);
    end
end

for i = 1:21
    for j = 1:21
        perr(i,j) = (Yvpcal(i,j) - Yvp(i,j))/Yvp(i,j);
    end
end

perr = 100*perr;
xp = x(1,:);
yp = y(:,1)';

figure(1)
mesh(xp,yp,Yvp), grid
xlabel('Nose Fraction')
ylabel('Mid-body Fraction')
zlabel('Yvprime')
view(60,30)
print -depsc2 yvp

figure(2)
mesh(xp,yp,perr), grid
xlabel('Nose Fraction')
ylabel('Mid-body Fraction')
zlabel('Yvprime Percent Error')
axis([.05 .25 .40 .60 -20 20])
view(60,30)
print -depsc2 yvperr

```

LIST OF REFERENCES

1. Papoulias, Fotis A., (1993) *Informal Lecture Notes for Marine Vehicle Dynamics ME 4823*, Naval Postgraduate School, Monterey, California
2. Wolkerstofer, William J., (1995) *A Linear Maneuvering Model for Simulation of Slice Hulls*, Master's Thesis, Naval Postgraduate School, Monterey, California
3. Naval Coastal Systems Center, *Evaluation of Semi-Emperical Methods for Predicting Linear Static and Rotary Hydrodynamic Coefficients*, NCSC TM-291-80, by R.S. Peterson, June, 1980
4. Naval Costal Systems Laboratory, *Prediction of Acceleration Hydrodynamic Coefficients for Underwater Vehicles from Geometric Parameters*, Naval Costal Systems Laboratory, NCSL-TR-327-78, by D.E. Humphreys and K. Watkinson, Febuary, 1978
5. Naval Coastal Systems Center, *Methods for Predicting Submersible Hydrodynamic Characteristics*, NCSC TM-238-78, by J. Fidler and C. Smith, Nielsen Engineering & Research Inc, July 1978
6. Hoerner, Sighard F., *Fluid Dynamic Drag*, 1965

INITIAL DISTRIBUTION LIST

	No. Copies
1. Defense Technical Information Center.....	2
8725 John J. Kingman Rd., STE 0944	
Fort Belvoir, Virginia 22060-6218	
2. Library, Code 13.....	2
Naval Postgraduate School	
Monterey, California 93943-5101	
3. Chairman, Code ME.....	1
Department of Mechanical Engineering	
Naval Postgraduate School	
Monterey, California 93943-5000	
4. Professor Fotis A. Papoulias, Code ME/PA.....	6
Department of Mechanical Engineering	
Naval Postgraduate School	
Monterey, California 93943-5100	
5. Naval Engineering Curricular Office, Code 34.....	1
Naval Postgraduate School	
Monterey, California 93943-5100	
6. LCDR Eric P. Holmes.....	2
111 Riverside Drive	
Newport News, Virginia 23606	